2020-09

RADAR-EMBEDDED SATCOM WITH DEEP NEURAL NETWORK DEMODULATION

Liu, Christopher Y.

Monterey, California. Naval Postgraduate School

NAVAL POSTGRADUATE SCHOOL

MONTEREY, CALIFORNIA

THESIS

RADAR-EMBEDDED SATCOM WITH DEEP NEURAL NETWORK DEMODULATION

by

Christopher Y. Liu

September 2020

Thesis Advisor: Ric Romero
Co-Advisor: Mark Karpenko

Approved for public release. Distribution is unlimited.

THIS PAGE INTENTIONALLY LEFT BLANK

REPORT DOCUMENTATION PAGE			*Form Approved OMB No. 0704-0188*

1. AGENCY USE ONLY *(Leave blank)*	**2. REPORT DATE** September 2020	**3. REPORT TYPE AND DATES COVERED** Master's thesis

4. TITLE AND SUBTITLE RADAR-EMBEDDED SATCOM WITH DEEP NEURAL NETWORK DEMODULATION	**5. FUNDING NUMBERS** W0A59
6. AUTHOR(S) Christopher Y. Liu	
7. PERFORMING ORGANIZATION NAME(S) AND ADDRESS(ES) Naval Postgraduate School Monterey, CA 93943-5000	**8. PERFORMING ORGANIZATION REPORT NUMBER**
9. SPONSORING / MONITORING AGENCY NAME(S) AND ADDRESS(ES) NPS Naval Research Program	**10. SPONSORING / MONITORING AGENCY REPORT NUMBER**

11. SUPPLEMENTARY NOTES The views expressed in this thesis are those of the author and do not reflect the official policy or position of the Department of Defense or the U.S. Government.

12a. DISTRIBUTION / AVAILABILITY STATEMENT Approved for public release. Distribution is unlimited.	**12b. DISTRIBUTION CODE** A

13. ABSTRACT (maximum 200 words)

In this work, the feasibility, design, and implementation of radar-embedded communications with satellite applications are investigated. We design a deep neural network (DNN) machine learning detector to demodulate SATCOM data. The performance result is compared with the detection method of using maximum likelihood estimation (MLE) to estimate the amplitude and phase of the radar signal, which is followed by a maximum likelihood detection (MLD) receiver. Pulsed radar and linear frequency modulation (LFM) waveforms are chosen to embed communications symbols. Quaternary phase-shift keying (QPSK) and eight phase-shift keying (8PSK) modulations are used for illustration. In this work, three DNN demodulators for radar-embedded communications are developed. One of the DNN detectors actually outperforms the MLD demodulator and is shown to be robust for pulsed radar-embedded communications. One of our goals is to embed satellite communications into LFM waveform, which is used in synthetic aperture radar (SAR). The DNN works well for LFM radar-embedded communications when the received LFM phase offset is removed a priori. However, the DNN symbol error rate (SER) performance suffers when the LFM phase offset is introduced for large RCR. Lastly, we perform laboratory transmission and reception tests: a) shielded cable and b) over-the-air (OTA) tests. It is shown that pulsed radar-embedded communication is feasible with both MLE-MLD and DNN detectors with reasonable SER performance.

14. SUBJECT TERMS SATCOM, RADAR, machine learning, radar-embedded comms, AI	**15. NUMBER OF PAGES** 67
	16. PRICE CODE

17. SECURITY CLASSIFICATION OF REPORT	**18. SECURITY CLASSIFICATION OF THIS PAGE**	**19. SECURITY CLASSIFICATION OF ABSTRACT**	**20. LIMITATION OF ABSTRACT**
Unclassified	Unclassified	Unclassified	UU

NSN 7540-01-280-5500 Standard Form 298 (Rev. 2-89) Prescribed by ANSI Std. 239-18

THIS PAGE INTENTIONALLY LEFT BLANK

Approved for public release. Distribution is unlimited.

RADAR-EMBEDDED SATCOM WITH DEEP NEURAL NETWORK DEMODULATION

Christopher Y. Liu
Lieutenant, United States Navy
BA, University of California – San Diego, 2002

Submitted in partial fulfillment of the
requirements for the degree of

MASTER OF SCIENCE IN ASTRONAUTICAL ENGINEERING

from the

NAVAL POSTGRADUATE SCHOOL
September 2020

Approved by: Ric Romero
Advisor

Mark Karpenko
Co-Advisor

Garth V. Hobson
Chair, Department of Mechanical and Aerospace Engineering

THIS PAGE INTENTIONALLY LEFT BLANK

ABSTRACT

In this work, the feasibility, design, and implementation of radar-embedded communications with satellite applications are investigated. We design a deep neural network (DNN) machine learning detector to demodulate SATCOM data. The performance result is compared with the detection method of using maximum likelihood estimation (MLE) to estimate the amplitude and phase of the radar signal, which is followed by a maximum likelihood detection (MLD) receiver. Pulsed radar and linear frequency modulation (LFM) waveforms are chosen to embed communications symbols. Quaternary phase-shift keying (QPSK) and eight phase-shift keying (8PSK) modulations are used for illustration. In this work, three DNN demodulators for radar-embedded communications are developed. One of the DNN detectors actually outperforms the MLD demodulator and is shown to be robust for pulsed radar-embedded communications. One of our goals is to embed satellite communications into LFM waveform, which is used in synthetic aperture radar (SAR). The DNN works well for LFM radar-embedded communications when the received LFM phase offset is removed a priori. However, the DNN symbol error rate (SER) performance suffers when the LFM phase offset is introduced for large RCR. Lastly, we perform laboratory transmission and reception tests: a) shielded cable and b) over-the-air (OTA) tests. It is shown that pulsed radar-embedded communication is feasible with both MLE-MLD and DNN detectors with reasonable SER performance.

THIS PAGE INTENTIONALLY LEFT BLANK

Table of Contents

THIS PAGE INTENTIONALLY LEFT BLANK

List of Figures

THIS PAGE INTENTIONALLY LEFT BLANK

List of Tables

THIS PAGE INTENTIONALLY LEFT BLANK

List of Acronyms and Abbreviations

A/D	analog-to-digital
AWGN	additive white Gaussian noise
BBV	base-band version
BER	bit error rate
C-SNR	communications signal to noise ratio
DNN	deep neural network
DoD	Department of Defense
LEO	low Earth orbit
LDA	linear discriminant analysis
LFM	linear frequency modulation
LPD	low probability of detection
LPI	low probability of interception
LSE	least squares estimator
ML	machine learning
MLD	maximum likelihood detection
MLE	maximum likelihood estimate
MLP	multi-layer perception
MFSK	multiple frequency shift keying
MPSK	multiple phase shift keying

MQAM multiple quadrature shift keying

NPS Naval Postgraduate School

OTA over the air

QDA quadratic discriminant analysis

QPSK Quaternary phase shift keying

RCR radar to communication ratio

RELU rectified linear unit

R-SNR radar signal to noise ratio

SAR synthetic aperture radar

SATCOM satellite communications

SER symbol error rate

SNR signal to noise ratio

SVM support vector machines

USN U.S. Navy

USG United States government

CHAPTER 1:
Introduction

Communications and sensing applications are ubiquitous in both the commercial and military domains. Low probability of detection or interception (LPD/LPI), as necessary function to military operations, has prompted the technique of embedding communications signals into radar transmissions [1].

Satellite communications (SATCOM), as the current primary method of communications for Naval ships, is critical; hence, we need to keep developing new ways of transmission while ensuring data security. Due to the high demands of SATCOM both domestically and internationally on the use of RF bandwidths, communications via satellites become competitive, congested, and contested.

Demodulation of wireless communications signals using optimal detectors such as maximum likelihood detection (MLD) and matched filters have been well understood and documented in the literature. However, the use of machine learning for effective demodulation of various communications signals is just starting to take hold [2]. Using deep neural networks can potentially yield better bit error rates (BER) and outperform other machine learning-based classifiers such as multilayer perceptron (MLP), support vector machines (SVM), linear discriminant analysis (LDA), quadratic discriminant analysis (QDA), and non-learning correlation-based demodulation methods similar to matched filtering [3]. This thesis compares the detection performance of machine learning demodulation (i.e., DNN) with match filtering demodulation (i.e., MLD) for radar-embedded communications.

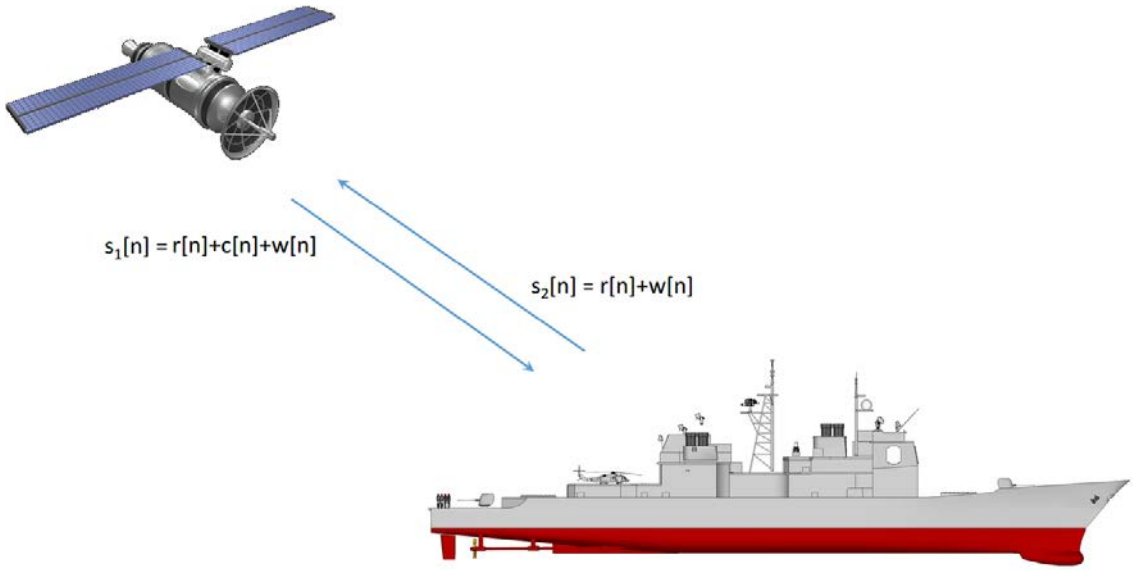

Figure 1.1. Space asset embeds communications c[n] in the radar signal r[n] to send data message to surface asset where w[n] is noise in the receiver

Higher-order modulation schemes, such as M-ary quadrature amplitude modulation (MQAM) and M-ary phase shift keying (MPSK) where M is greater than 4, are spectrally efficient as opposed to M-ary frequency shift keying (MFSK) but do not perform well when the received energy is low [4]. This is an issue that can potentially be mitigated with the help of machine learning demodulation. This thesis employs low energy MPSK modulated communications signals to integrate with high-energy radar signals and utilize machine learning to demodulate the relatively low powered communications data.

This research provides a design to test the suitability and feasibility of machine learning for actual Naval/Joint communications missions. This work directly supports future payload applications for satellite communications and electronic warfare. As shown in Figure 1.1, it may expand the capabilities for LPI satellite communications. Moreover, it may also lead to efficient bandwidth use and therefore less electromagnetic interference. It may also provide new SATCOM frequency band options and flexibilities.

Almost all satellites have payloads for communications and sensing systems including radar, e.g., synthetic aperture radar (SAR). The Air Force proposed space radar system with a constellation "envisioned to consist of nine satellites, providing worldwide coverage with

a frequent revisit rate" and carrying synthetic aperture radar onboard [5]. If combined with the radar embedded communications capability, not only would world-wide radar imagery be possible, it would also be possible to communicate at the same time within the same allowed frequency band. Of course, the feasible data rate is constrained by the radar bandwidth available.

This new type of communications has very interesting advantages. First, the embedded communications is low-power and thus have LPI quality. Second, the use of same frequency bandwidth along with the radar at the same time utilizes the satellite RF spectrum efficiently. Third, it presents cost-saving benefits.

Table 1.1. Link budget calculation for radar embedded communications from a satellite in LEO orbit

	Magnitude	Unit
Transmit Power (@ 5 Watt)	37.0	dBm
Cable Loss	1.0	dB
Transmit Antenna Gain	6.0	dB
EIRP	42.0	dBm
Slant Range	1695	km
Free Space Loss	176.1	dB
Bit Rate	100000	bps
Noise kT	-174.0	dBm/Hz
Receiving Antenna Gain	25.0	dB
Received SNR FE	13.9	dB
Noise Figure	2.0	dB
Bandlimiting Loss	0.0	dB
Implementation Loss	1.5	dB
Achieved Eb/No	10.4	dB
Required Eb/No	9.5	dB
Link Margin	0.9	dB

Typical satellite performs radar functions dwells in LEO orbits, which usually ranges

between 150 to 1000 km. To compute the link budget (Table 1.1) for a satellite to perform radar embedded communications, we set the altitude of the spacecraft at 500 km, with an elevation angle of 10 degrees. Considering SAR frequency range onboard satellites, the transmitting frequency is set at 9 GHz. The transmit power here is for the communications signal. Using RCR desired, the radar power can easily be computed.

The novelty of this work is the application and development of DNN detectors to radar-embedded communications waveforms. Our goal in this work is to achieve a new way of satellite communications through embedding of communications transmissions within the radar signals. This goal is coupled with new detection techniques which include machine learning methods and traditional methods. This thesis uses Monte Carlo simulation methods to report detection performance of this new embedded SATCOM technique. Symbol error rates (SER) for QPSK and 8-PSK with the use of MLE-MLD and the new DNN detection methods are reported in the following chapters.

CHAPTER 2:
Signal Model and Radar Estimation

To integrate the communications signals into radar transmissions, this thesis follows and summarizes the approach in [6] using superposition of a communications signal to a high-powered radar signal. Amazingly, the high power constraint to the radar signal is not necessary for both the traditional and machine learning detectors to work, as long as the techniques are coupled by MLE of the radar's complex-valued baseband amplitude. Stated simply, data symbols employing QPSK modulation are embedded into high-powered radar transmissions.

As shown in Figure 2.1, the embedded communications signal become more apparent as the radar to communications ratio (RCR) decreases. Therefore, in order to achieve more LPI quality, the greater the RCR is, the less evident the communications signal would be in Figure 2.1. The value of RCR is critical for training and test simulations of the machine learning demodulators in Chapter 3. RCR is given by [7]

$$RCR = \frac{P_r}{P_c}, \tag{2.1}$$

where P_r is the power of the radar signal and P_c is the power of communications signal.

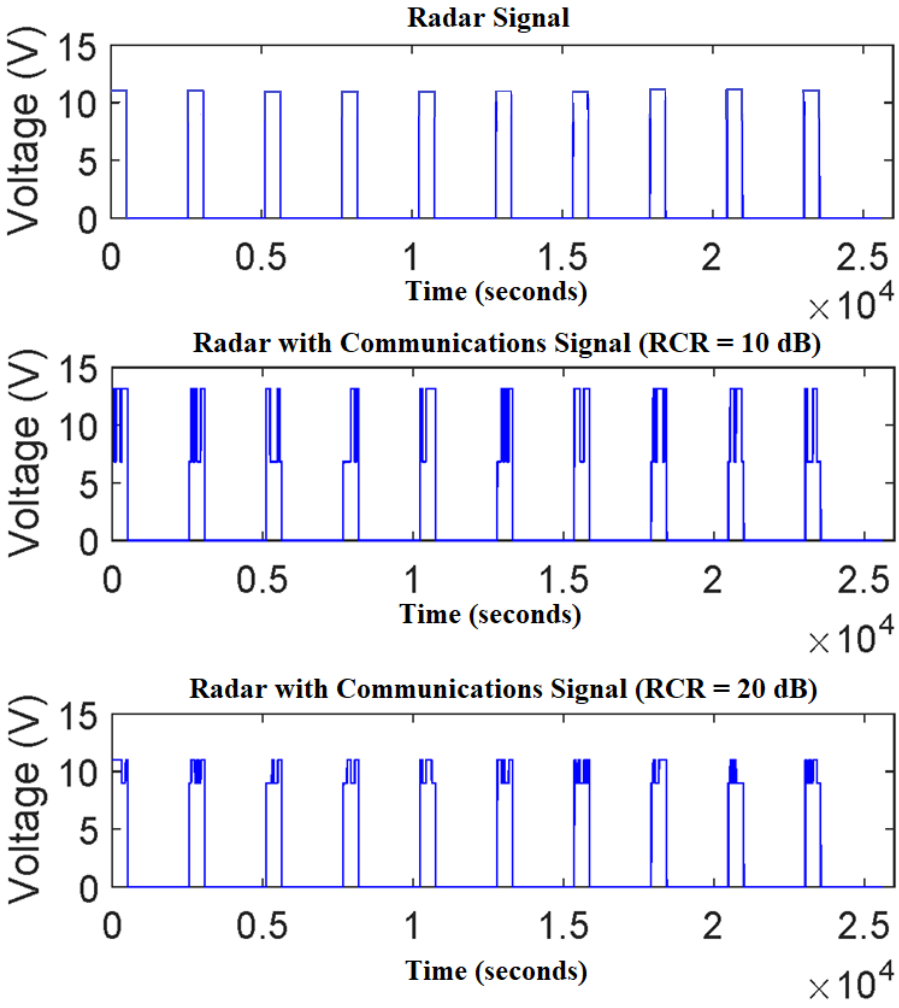

Figure 2.1. An example of pulsed radar waves with communications signal embedded at different radar-to-communications ratio. Adapted from [7].

2.1 Signal Model

A complex-valued baseband signal model for the radar-embedded communications signal is utilized here, such that the signal received at the communications receiver is: $y(t) = r(t) + c(t) + w(t)$, where $r(t)$ is the radar signal, $c(t)$ is the communications signals, and $w(t)$ is the additive white Gaussian noise (AWGN) or the thermal noise in the receiver.

Signal processing occurs after analog-to-digital (A/D) sampling, where we assume a discrete signal model with sampling frequency at least twice the Nyquist frequency [8].

Additionally, normalized sampling time is employed, where $T_s = 1$; therefore the vector model for the received signal is given by

$$\mathbf{y} = \mathbf{r} + \mathbf{c} + \mathbf{w}, \tag{2.2}$$

where $\mathbf{r}$, $\mathbf{c}$, and $\mathbf{w}$ are the received radar, communications, and noise vectors respectively [6]. Let the radar signal model have amplitude A, with possible phase offset ϕ_r, where the radar complex-valued baseband signal (one-sample vector) is given by

$$\mathbf{r} = Ae^{j\phi_r}. \tag{2.3}$$

The communications symbols are randomly generated, where the QPSK symbol phases are given by $\phi_q \in [\frac{\pi}{4}, \frac{3\pi}{4}, \frac{5\pi}{4}, \frac{7\pi}{4}]$ [6]. If the magnitude of a QPSK symbol is Q, then the communications (one-sample) vector is given by

$$\mathbf{c} = Qe^{j\phi_q}. \tag{2.4}$$

The AWGN $\mathbf{w}$ is modeled as complex, additive, and normally distributed noise with sample variance σ^2 [6]. If the symbol rate of the communications signal is higher than the bandwidth of the radar signal, then there are potentially more communications samples in one radar pulse. If so, Equations 2.2 to 2.4 can easily be extended.

2.2 Pulsed Radar Estimation and Detection

One of the most utilized radar in today's commercial and military applications is the pulsed radar. The radar-embedded communications modeling is started with this type of radar. Of course, the amplitude and phase may be known to the radar transmitter. However, as a receiver of the radar embedded communications, the phase is not necessarily known since it may be a function of many propagation effects, the least of which is the distance traveled by the waveform. As pointed out in [6], employing MLD for symbol demodulation directly does not work effectively since the radar signal becomes a large power interference in the communications receiver. Indeed, employing MLD without accounting for the received radar phase yields a QPSK SER approximately close to 0.75 at low communications SNR. Thus, MLE of radar amplitude (with long collection time) for subtraction prior to MLD

improves the SER significantly.

Normalized symbol duration is assumed ($T_s = 1$ as indicated before). Let E_q be the average energy of the communications symbol and let N be the number of symbols in which the radar magnitude and phase are to be estimated inside a pulse. In the radar transmitter, the radar phase is designed to be constant (ϕ_r) and/or it can be co-phased with the communications symbols since the symbols are embeded in the radar waveform directly and thus the effective phase differential is simply (ϕ_r). However, this (differential) phase is not assumed to be known in the communications receiver, which is what happens in practice; thus there is a need to estimate not only the unknown received phase but also the magnitude of the radar signal such that interference subtraction can be performed. The block diagram for this procedure is shown in Figure 2.2.

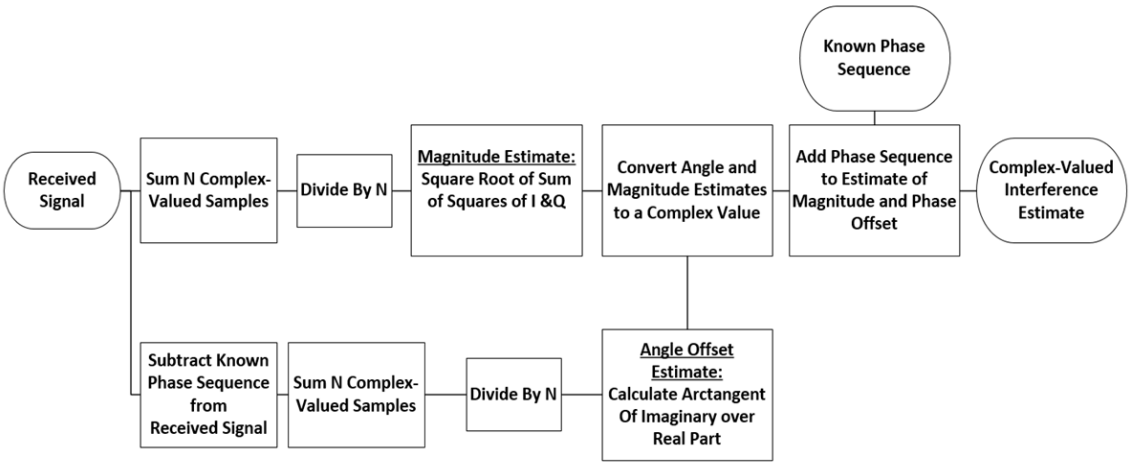

Figure 2.2. The procedure to collect N symbols in a pulse and estimate radar amplitude and phase offset in order to demodulate communications signals. Source: [9].

Since the radar amplitude is much greater than that of the communications signal, it can be shown that the MLE of the radar amplitude is approximated by $\hat{\mathbf{r}} = \mathrm{E}[\mathbf{y}]$ where $\mathrm{E}[\cdot]$ is the expected value operator. Since the radar amplitude is assumed to be constant at least when N symbols are embedded and used for estimation, the variance of the estimate can also be approximated by [6]

$$\mathrm{var}(\hat{\mathbf{r}}) = \frac{E_q + \sigma^2}{N}. \tag{2.5}$$

As noted in [6], the variance of the estimate decreases as N increases. Also, notice that the variance of the estimate is increased by the average energy of the communications signal. In other words, in order to decrease the estimated variance, E_q needs to decrease; but decreasing it too much may render communications SNR to be too low. In other words, there is an inherent contrasting desire to embed communications signal and minimize the radar interference in view of detecting the communications signal with acceptable SER.

In signal processing, the radar magnitude estimate is calculated by taking the square root of the sum of the squares of the real and imaginary parts of the complex estimate $\hat{\mathbf{r}}$. The phase is calculated by taking the arctangent of the ratio of imaginary part of $\hat{\mathbf{r}}$ over the real part of $\hat{\mathbf{r}}$.

2.3 LFM Radar Estimation and Detection

Linear frequency modulated waveform has been utilized since World War II. The once classified LFM waveforms are now heavily utilized in modern military and commercial radars due to its unique properties that enables radars to search, track, and achieve high-resolution modes. LFM system is the second type of radar that will be utilized in this radar-embedded communications research. The LFM waveform is a sinusoidal waveform where its frequency changes linearly in time. A baseband LFM pulse is given by

$$x(t) = A\cos\left(\pi\frac{B}{\tau}t^2\right), \qquad -\frac{\tau}{2} \leq t \leq \frac{\tau}{2}. \tag{2.6}$$

where A is the amplitude, B is the bandwidth, and τ is the duration of the pulse [10]. Once the LFM baseband is formulated, the same approach described in Section 2.2 can be followed. By adding the QPSK communications vector, the noise vector, and this time with the LFM radar vector, the receiver LFM radar embedded communications signal is easily formed. However, the same challenge of estimating the LFM signal amplitude or energy as well as the phase offset exist. Going back to the vector formulation where $T_s = 1$, let $\mathbf{r_x}$ be the received signal, where the radar energy E_e can be estimated in a pulse duration with

$$E_e = \sum |r_x[n]|^2. \tag{2.7}$$

For the phase offset estimation, it is not quite as straightforward as simply averaging as in the case rectangular radar pulse with a phase offset. In our formulation, the phase angle Ph_t is estimated from the sum of the received signal and compared with angle Ph_b , which is the phase of the summed LFM baseband signal. The phase offset Ph_e is estimated with

$$Ph_e = Ph_t - Ph_b. \tag{2.8}$$

With both the radar energy and phase offset calculated, the estimated baseband version (BBV) of the LFM waveform is obtained. The BBV is then subtracted from the received signal which yields the residue that contains both communications signal plus noise. MLD is used for detection. The result is then compared with the original data to evaluate SER. The machine learning demodulation will be discussed in Chapter 3.

CHAPTER 3:
Neural Network and Monte Carlo Simulations

While various machine learning techniques are feasible, deep neural networks (DNN) is chosen to perform the detection of radar-embedded communications. The deep learning process significantly reduces the complexity of network connections in the neural network and can reduce the number of parameters necessary to be learned by the network. The same kernel is applied across the received signal. Each value of the output signal feature is created by a small subset of the input data equal to the size of the kernel. By definition, DNN consists of an input layer, the hidden layers, and an output layer. After repetitive trials and remodeling, it is found that with three hidden layers, 16 nodes per layer, and Rectified Linear Unit (ReLU) as the activation function yield the best results for this task within reasonable time.

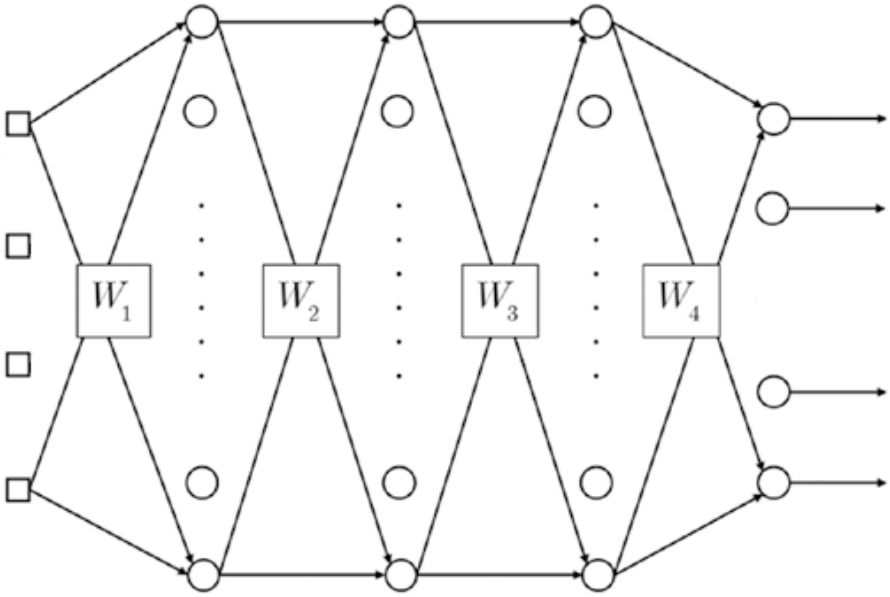

Figure 3.1. Deep neural network design for this application. Adapted from [11].

The ReLU converts all negative values to zero from the neural network layer, which helps to emphasize the features from each layer and the features selected during the pooling

of the next layer. At the last layer, the network is terminated with the Softmax function as our symbol classifier. The activation functions ReLU and Softmax are given mathematically by [12]

$$ReLU(\mathbf{x}) = \max(0, \mathbf{x}) \tag{3.1}$$

$$Softmax(\mathbf{x}) = \frac{e^{\mathbf{x}}}{\Sigma e^{\mathbf{x}}}. \tag{3.2}$$

After training the neural network and obtaining the machine learning demodulated result (via DNN), it is compared with the original data to calculate the detection performance, which is then compared with the MLE-MLD performance by plotting their corresponding SER curves. The simulation procedures in MATLAB for MLD and DNN demodulation methods are shown in Figure 3.1 and Figure 3.2, respectively.

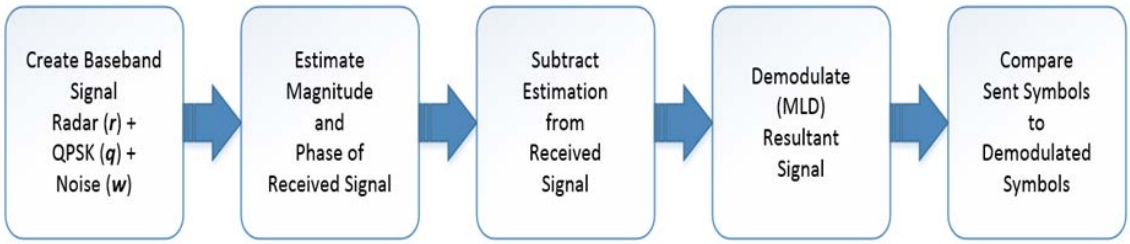

Figure 3.2. The Monte Carlo simulation procedure for MLD demodulation. Source: [9].

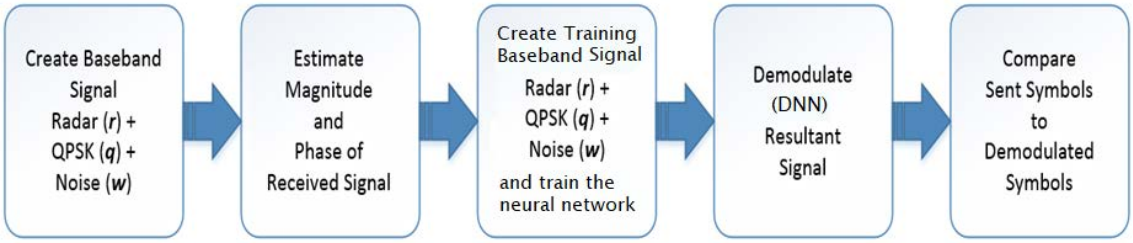

Figure 3.3. The Monte Carlo simulation procedure for DNN demodulation

3.1 Training the DNN

For training, 5000 data symbols are randomly generated, modulated into PSK format, and utilized in supervised training of the DNN, i.e., the DNN is trained with the

randomly generated communications data symbols in order to learn how to correctly demodulate/detect the symbols. Once the training is complete, a new set of random communications data is generated for transmission and embedded into the radar signal to test the machine learning detection, which is achieved through backpropagation. In backpropagation, we use the loss function and propagate errors backwards through the network adjusting weights and bias to minimize the loss [12]. The updated DNN weight (**W**) and bias (**b**) with backpropagation for activation output are shown in the equations below:

$$\mathbf{W}^n(k+1) = \mathbf{W}^n(k) - as^n(a^{n-1})^T, \tag{3.3}$$

and

$$\mathbf{b}^n(k+1) = \mathbf{b}^n(k) - as^n, \tag{3.4}$$

where a is the number of nodes, n is the number of hidden layers, sensitivity s, example k, and T indicates the transpose operation [12].

Through training and testing of DNN, an interesting phenomenon is observed. In the Monte Carlo simulations, even though the received signal SNR is varied to be different values, the machine learning demodulation results are always better when the DNN is trained with QPSK modulation when SNR is about 4 dB.

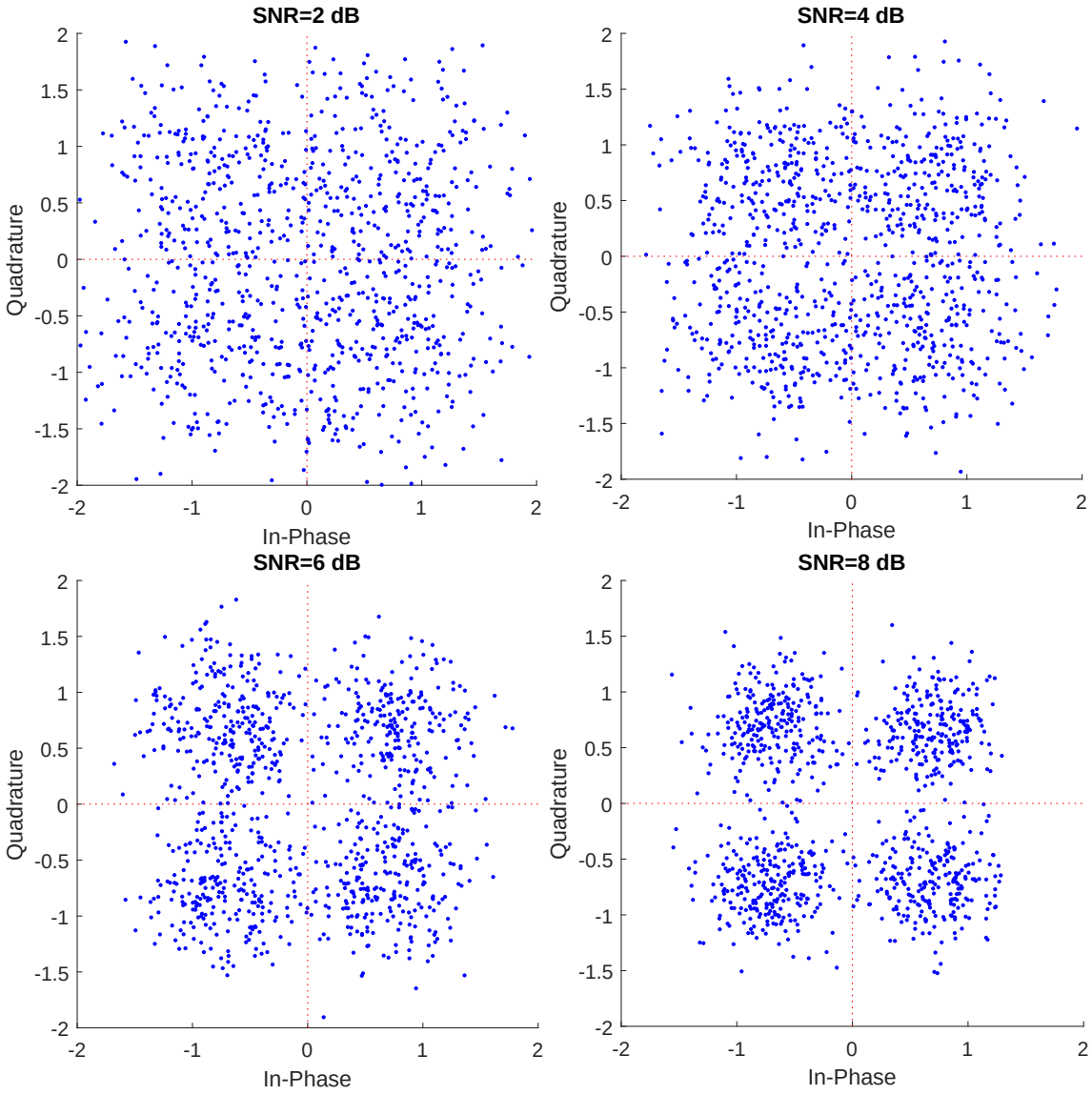

Figure 3.4. QPSK modulated 5000 randomly generated data points for machine learning training at different SNRs

This interesting result is intuitively unexpected. Perhaps an insight can be gained by plotting the symbol constellations plots of the QPSK training set for increasing SNR. The symbol constellations for SNR = 2, 4, 6, and 8 dB are shown in Figure 3.1. Visually, a

relatively high SNR = 8 dB (or even larger) seems like a good training value. It turns out that noise itself is critical to training the DNN demodulator, which is against conventional detectors that desires noise to be minimized for optimum detection.

As shown in Figure 3.4, at SNR = 6 dB and above, there is usually not enough noise in the training data in order to properly train the DNN. On the other hand, if the DNN is trained at SNR = 2 dB or below to increase the noise energy relation to symbol energy, the constellation plot seems to tilt the constellation mean to zero instead of the symbols' amplitudes in the 4 quadrants for QPSK modulation. This gives an important insight as to why high SNR or low SNR does not work for training DNN and why only moderate SNR seems best. Interestingly, in our extensive simulations, the each training data SNR is set to the exact matching SNR in the test data, but somehow the demodulation SER results are still not as good as simply setting the training SNR to 4 dB.

3.2 DNN Demodulation and Results

To extract communications data from radar transmissions, the initial approach is to estimate the radar magnitude and phase offset. After the radar parameters are estimated, it can be subtracted from the received signal to mitigate out the radar interference. Then, the resulting signal is taken to perform machine learning demodulation to obtain the communications data. Monte Carlo simulation is employed to generate SER curves as a function of communications signal-to-noise ratio (C-SNR). C-SNR is specifically used to differentiate it from radar signal-to noise ratio (R-SNR) [6].

3.2.1 DNN Demodulator ver.1

For our first version of machine learning DNN demodulator, the communications signals are extracted from the radar transmission by subtracting the radar signal via its estimated parameters from the received signal. Since the radar is assumed to be high powered, the radar-to-communications power ratio (RCR) is set to 20 dB. Then as mentioned in Section III, 5000 noise-corrupted modulated radar-embedded communications symbols are used to train the DNN. The DNN demodulator performance is compared to MLE-MLD demodulator, where the radar estimate is subtracted prior to detection. The SER results as function of increasing symbol samples N are shown in Figure 3.5.

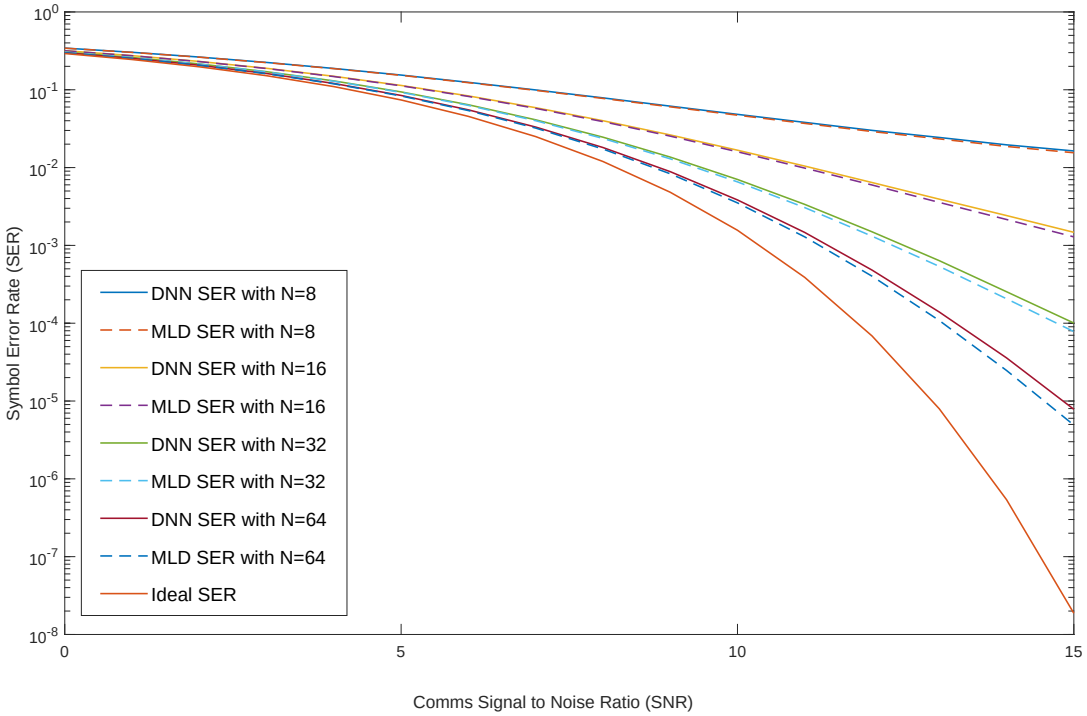

Figure 3.5. SER results of DNN and MLD demodulators after radar parameter MLE and subtraction (DNN demodulator ver.1)

As shown in Figure 3.5, both the machine learning and MLD demodulation are affected by the collection time N as may be expected. The SER curves for both demodulation methods approach the theoretical ideal SER for QPSK demodulation as the collection time increases. This is because the longer the collection time, the better are the estimate of the radar parameters.

Both methods perform well and the SERs are very close with the MLE-MLD performing slightly better than DNN when N is large.

3.2.2 DNN Demodulator ver.2

In the second version of the machine learning demodulator, the machine is trained with the raw received signals (i.e., without subtracting the estimated radar parameters). The MLE of radar amplitude and phase shift are used as training inputs for the neural network.

Again, RCR is set to 20 dB and the SER results are shown in Figure 3.6.

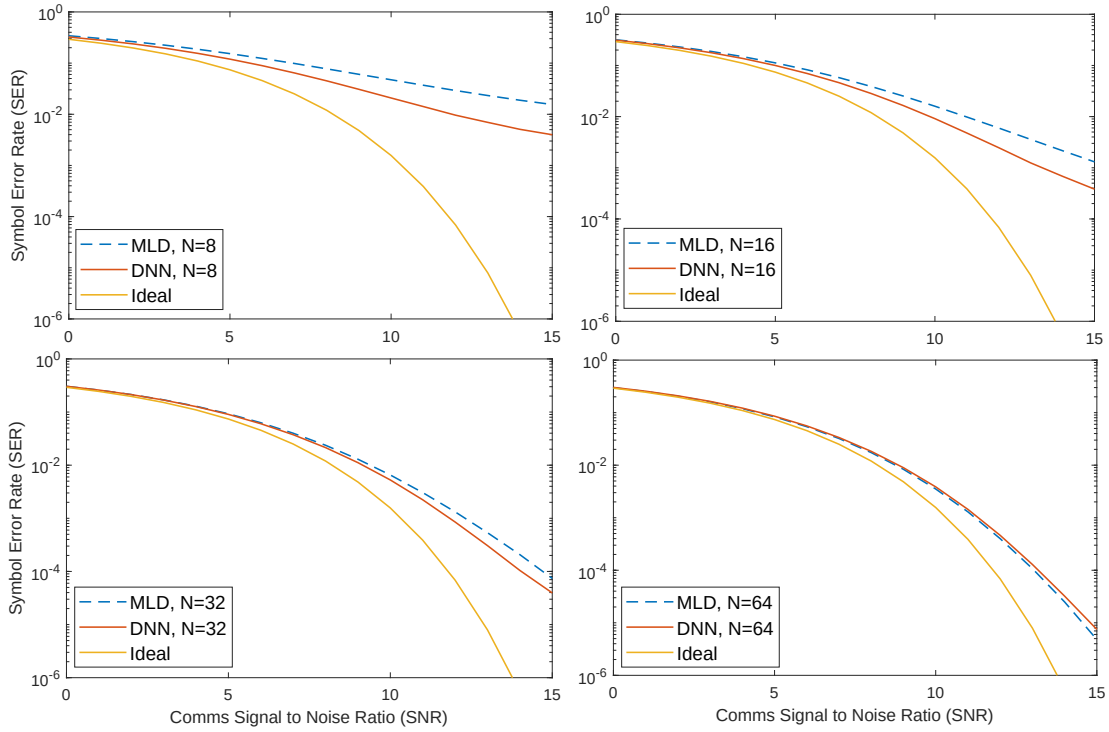

Figure 3.6. SER results of MLE-MLD demodulation vs. DNN demodulation with radar estimation as training input (DNN demodulator ver.2)

As shown in Figure 3.6, SERs for both the MLD and DNN are still very close to each other and obviously improve as N increases. However, the DNN demodulator outperforms the MLE-MLD demodulator at lower collection times. This is important for latency-limited applications. It means that the DNN demodulator performs better for real-time applications which is desirable in several wireless applications.

3.2.3 DNN Demodulator ver.3

In the third version of the machine learning demodulator, the goal is to explore the effect of decreasing RCR. Such an experiment is worthy of investigation. This is because in [5], [6], it was shown that the MLD detector (as long as MLE and radar subtraction are employed) performed very well regardless of RCR. If machine learning is to be used as a

viable radar-embedded communications receiver, then it also has to be robust for changing values of RCR. The DNN is again trained with raw received signal and radar estimates as machine learning inputs for various RCR values. Through extensive machine learning testing and simulations, it is found that a near ideal RCR value exist for the DNN to train on such that its detection performance is robust for various RCR.

For robustness, a large deviation of values of RCR are used: 20, 10, 0, -10 dB. Similar to the near ideal C-SNR ratio (= 4 dB) for DNN training with noise, an RCR training value of 28 dB is identified to make the DNN demodulator robust for any variation for RCR. The SER results for RCR = 20 dB in shown in Figure 3.7.

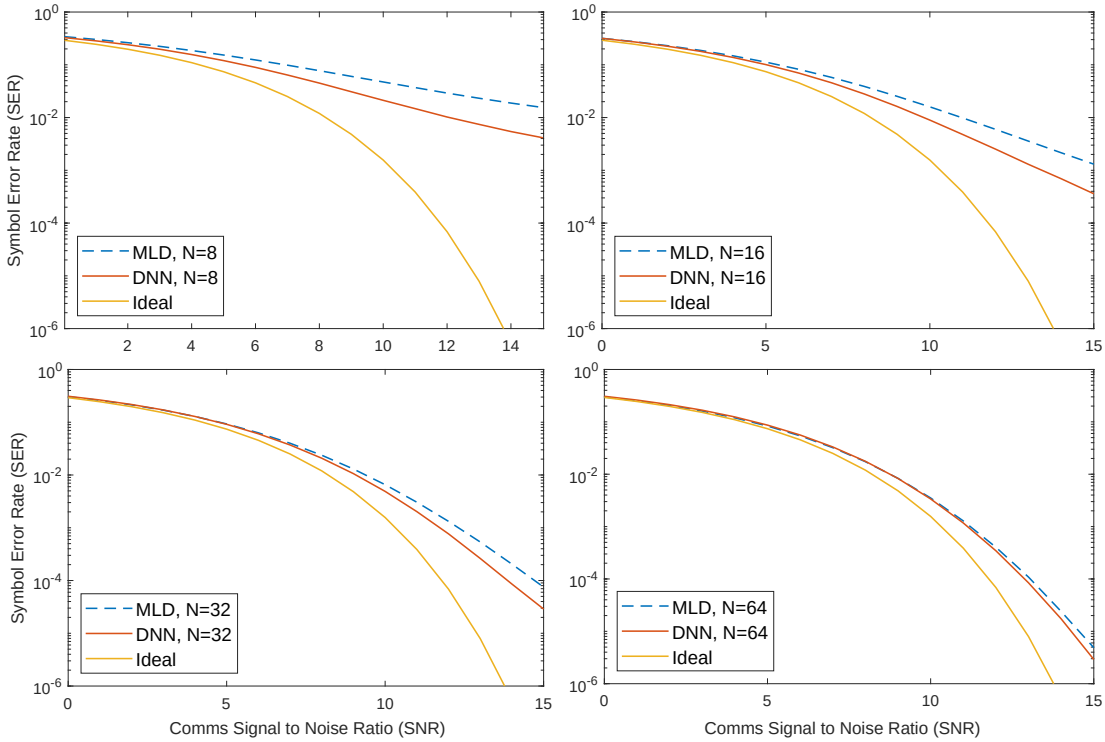

Figure 3.7. SER performance curves of MLE-MLD demodulation vs. DNN demodulation with radar estimation as training input and application of near ideal RCR in DNN training (DNN demodulator ver.3)

As shown in Figure 3.7 that DNN demodulator outperforms the MLE-MLD detector at every collection time *N*. The same simulations are tested at RCR = 10, 0, -10 dB using the

trained DNN at RCR = 28 dB. The SERs are very similar to Figure 3.7. In other words, the DNN demodulator is very robust just like the MLE-MLD; however, the machine learning DNN actually outperforms MLE-MLD! (For brevity, not all SER curves are shown for RCR = 10, 0, and -10 dB).

3.3 8-PSK DNN Demodulation

Utilizing DNN demodulator ver.3, the neural network is modified to work with an 8PSK modulated communications embedded in pulsed radar signals. It is investigated if MPSK machine learning demodulation has a near ideal C-SNR and RCR for the machine learning training process as observed before. First, the near ideal C-SNR has to be identified to generate the training data for the DNN. Just like in the case of QPSK as illustrated in Figure 3.1, the SNR has to be dialed such that the DNN detector is trained with proper amount of noise power in relation to the 8 constellation points for proper demodulation.

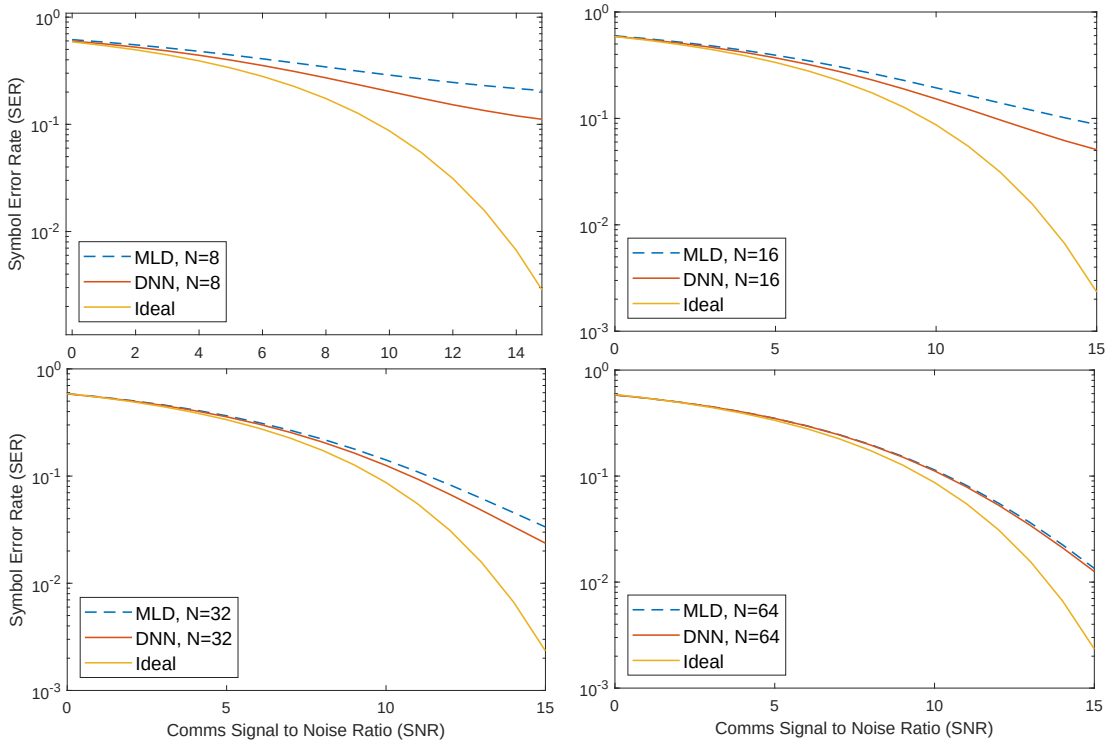

Figure 3.8. SER performance curves of MLD demodulation vs. DNN demodulation with radar estimation as training input, and application of near ideal RCR in DNN training with 8PSK signals

Through repeated simulations while varying the SNR and RCR of the training data, the near ideal C-SNR is found for training the neural network, which is 10 dB while the near ideal RCR is 30 dB for 8-PSK symbols embedded in pulsed radar signals.

As shown in Figure 3.8, SER result from machine learning demodulation outperforms the MLE-MLD detector at all tested symbol lengths. Furthermore, it confirms that for MPSK communications embedded in radar signals, there are near ideal C-SNR and RCR values that can be used to train the machine for near-optimal DNN demodulation performance.

3.4 LFM DNN Demodulation

In this section, the QPSK modulated communications symbols and noise are embedded into the LFM radar signal in the simulations as usual. Again the DNN demodulator ver.3

is used to demodulate the communications symbols from the LFM waveform. Utilizing the same parameters for comparison, the number of communications symbols N_s is set to 8, 16, 32, and 64.

Having identified the near ideal SNR and RCR for training the neural network to demodulate pulsed radar embedded communications from before, effort is made to identify the optimal SNR and RCR for training the neural network for near optimal demodulation results. However, unlike the pulsed radar signals, the IQ plot for LFM embedded communications does not resemble standard phase-modulated communications symbols. This makes it much harder to identify a range of SNR and RCR to start training the neural network with.

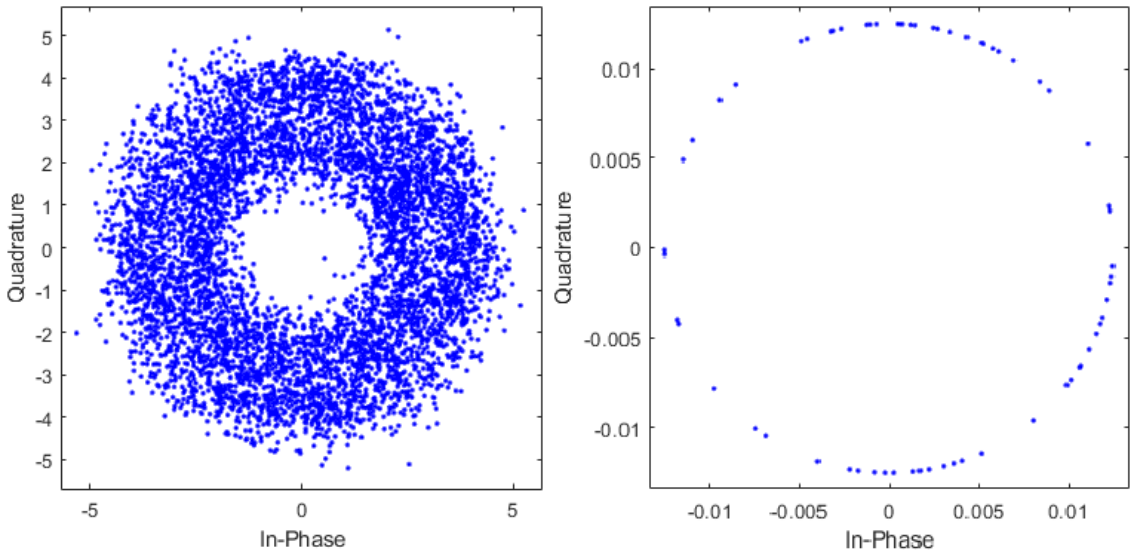

Figure 3.9. QPSK modulated 6400 randomly generated data points embedded in LFM waveform (left), and LFM baseband (right) for machine learning training

To train the neural network, 6400 QPSK symbols are randomly generated and embedded into the baseband LFM waveform as shown in Figure 3.9. A good initial approach to test both MLD and DNN detectors is to exclude the phase offset to the LFM signal while embedding the QPSK symbols. The MLD vs DNN demodulation SER is shown in Figure 3.10.

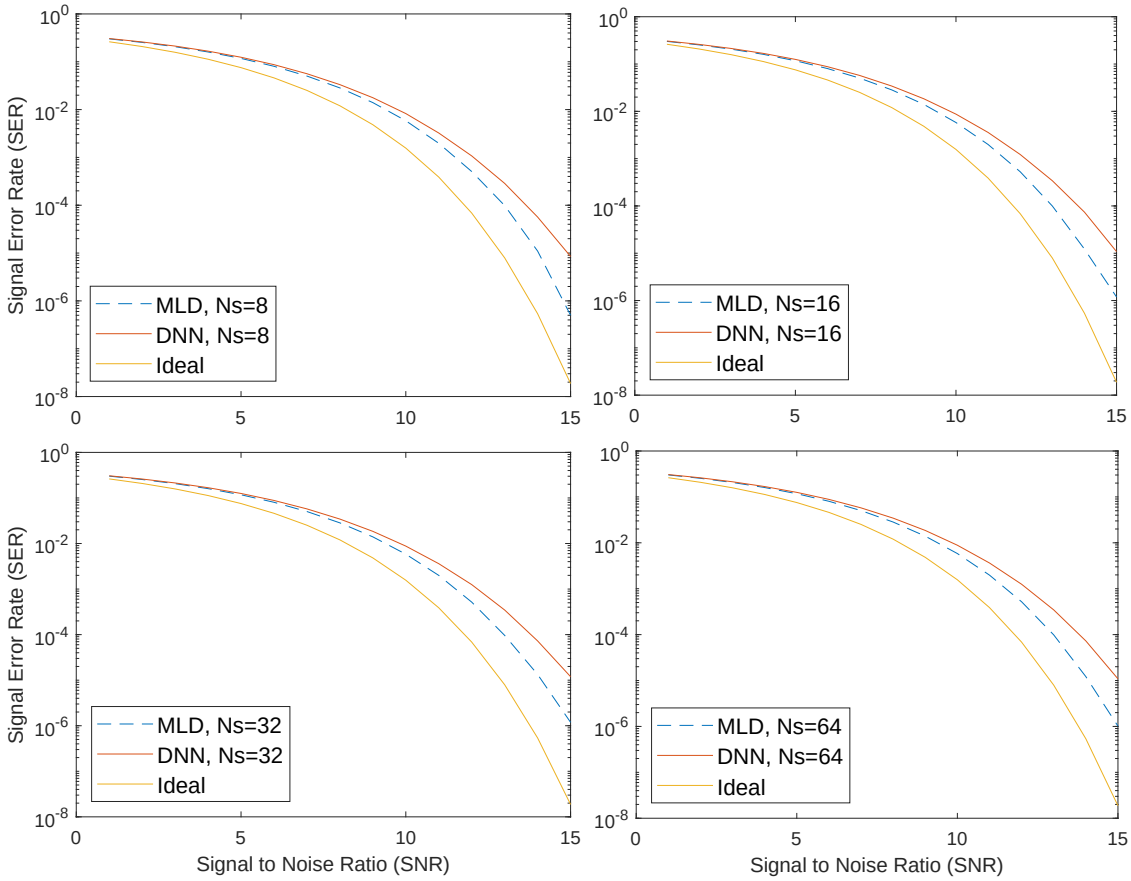

Figure 3.10. SER performance curves of MLE-MLD vs DNN demodulation for LFM radar embedded comms simulation ver.1 (without radar phase offset)

As shown in Figure 3.10, the MLD demodulator performs better than the DNN demodulator in this simulation. Nonetheless, the results also show that our DNN design does work for demodulating LFM embedded communications. It is also notable that due to the nature of LFM being a continuous wave, changing the amount of communications symbols embedded in the LFM radar does not change the demodulation performance (which is a phenomenon to be scrutinized later).

After showing both methods to demodulate LFM embedded communications, practical issues are now introduced into the simulations. Two issues are unknown: receive phase offset and RCR variations on the simulated signals.

In the second round of simulations, the LFM phase offset is integrated into the

received signal. The estimated LFM baseband phase-shift is subtracted from the received raw signal for MLD demodulation. As for the DNN demodulation, the neural network is given both the received raw signal and the estimated baseband parameters based on separately generated random data for ML training.

Through extensive simulations, it is found that when RCR is set to 10 dB, and SNR set to 8 dB for ML training, the DNN produces good results (no phase offset case). This time, instead of varying the numbers of communications symbols embedded in the LFM waveform, 500 symbols are embedded into all four iterations of simulation as shown in Figure 3.11, with RCR set to -10, 0, 10, and 20. The Monte Carlo simulations are performed to produce SER with different RCRs.

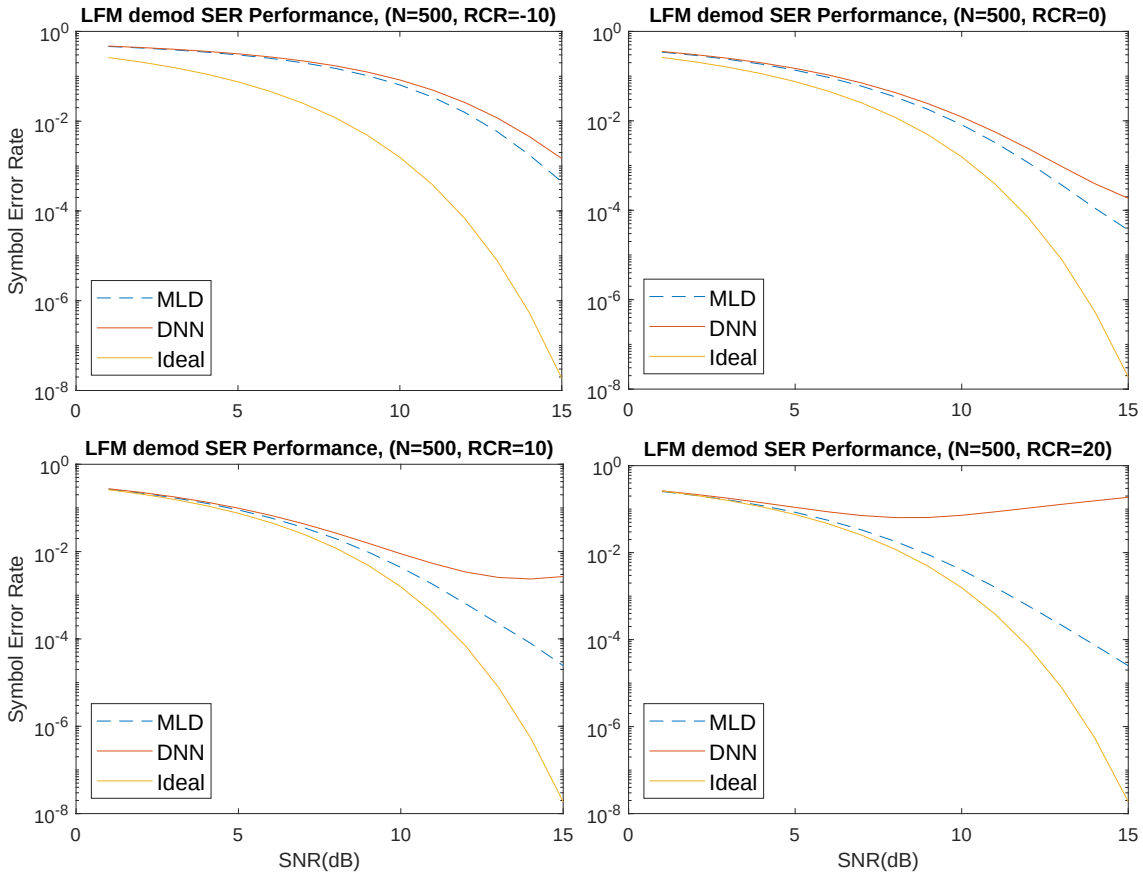

Figure 3.11. SER performance curves of MLE-MLD vs DNN demodulation for LFM radar embedded comms simulation ver.2 where LFM is received with phase offset

As shown in Figure 3.11, the estimation and subtraction of phase offset coupled with MLD work well as a LFM radar-embedded communications detector. However, for machine learning, it appears that the current DNN design does not perform well for large RCR with the unknown phase offset for LFM radar-embedded communications. The DNN SER performance worsens as the RCR is increased. Various changes of the DNN designs to the numbers of nodes and hidden layers are executed with similar degraded SER results at large RCR. If the baseband amplitude and phase estimates are subtracted from the received signal for DNN, then its performance is much better compared to the SER curves shown in

Figure 3.11, but the results are still slightly worse compared to the MLD demodulator as seen in Figure 3.10.

3.4.1 LFM demodulation with MATLAB Machine Learning Toolbox

It is known that MATLAB (as well as various machine learning sofware) has its own built-in machine learning functions. It is decided to incorporate MATLAB's machine learning functions in the LFM demodulator. The hope is to utilize MATLAB's various optimizer functions to improve DNN SER performance when a LFM phase offset is present.

With the newly written DNN detector using MATLAB's machine learning function structures, the data generation, machine learning training, and the testing portions are able to be separated, which greatly saves processing time. Through trials and errors, it is found that the optimizer function performs the best in demodulating radar-embedded communications is the Adam optimizer function.

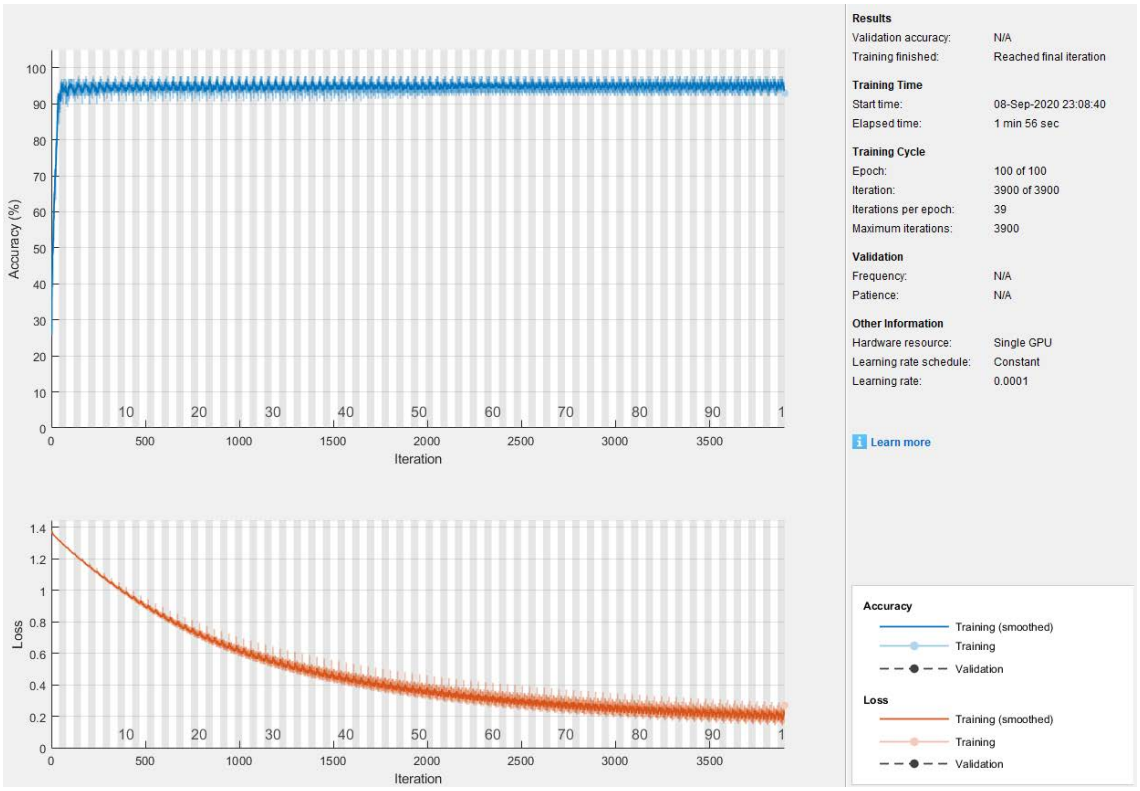

Figure 3.12. DNN performance with MATLAB built-in ML functions for pulsed radar embedded communications

However, the performance of the newly written DNN with MATLAB's built-in functions is actually subpar compared to our previously designed DNN demodulators. The percentage of correct symbol decision of the new DNN peaks around 87 to 89 percent with pulsed radar embedded communications even with the Adam optimizer function. In other words, SER is around 0.12, which is unacceptable. After lengthy attempts and various configurations using MATLAB's built-in machine learning functions and optimizers, its SER performance still doesn't match our original DNN detectors. Thus, the MLE-MLD and the original DNN detectors are used in the laboratory over-the-air testing in Chapter 4.

Looking into the original DNN codes, although machine learning optimization is not written separately as an "optimizer function" as in conventional machine learning programming, the cost function is calculated and coded based on the optimization theory. As with most neural network ML training, the cross entropy approach is taken for the

superior performance and learning rate [11], which results in the better performance of demodulating radar embedded communications when compared to the MATLAB built-in ML functions.

CHAPTER 4:
Laboratory Test Results

In this chapter, we discuss physical signal generation of the pulsed radar and LFM radar waveforms with QPSK communications symbols embedded in the laboratory. It is our objective to show that our detectors work in practice with the actual generation and reception of physical signals via shielded cable and over-the-air (OTA) transmissions.

The transmitting equipment used in the laboratory is the Rohde & Schwarz SMW200A Vector Signal Generator (SigGen) with frequency range up to 3 GHz to replicate satellite communications frequencies ranges. R&S FSW Signal & Spectrum Analyzer (SpecAn) with frequency range up to 8 GHz is used as the receiving equipment and received signal samples are transferred to a laptop or computer for post-processing.

4.1 Pulsed Radar Embedded Communications Test

4.1.1 Shielded Cable Transmission Test

To conduct the physical text, we first need to generate actual radar embedded QPSK comms signals. To easily identify the communications sequence for post processing of received data, 100 zero-constellation symbols are inserted in the beginning of the communications data as marker with 4900 randomized QPSK symbols generated for total of 5000 communications symbols to be embedded into the pulsed radar waveform. We set RCR = 10 dB and SNR = 20 dB initially to produce the .wv file from MATLAB (Figure 4.1). The .wv file is then loaded into the SigGen for physical signal generation. It should be noted that the SpecAn has a has a spec noise figure (NF) of $\leq$ 14 dB. Our estimate is that it has an actual NF = 12 dB and thus the effective received SNR is actually 8 dB.

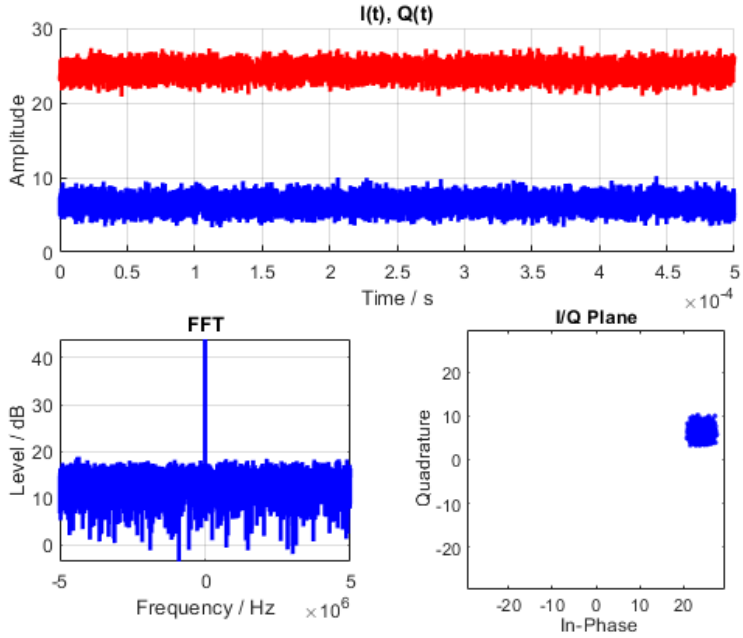

Figure 4.1. Producing pulsed radar embedded communications .wv file for physical signal generation.

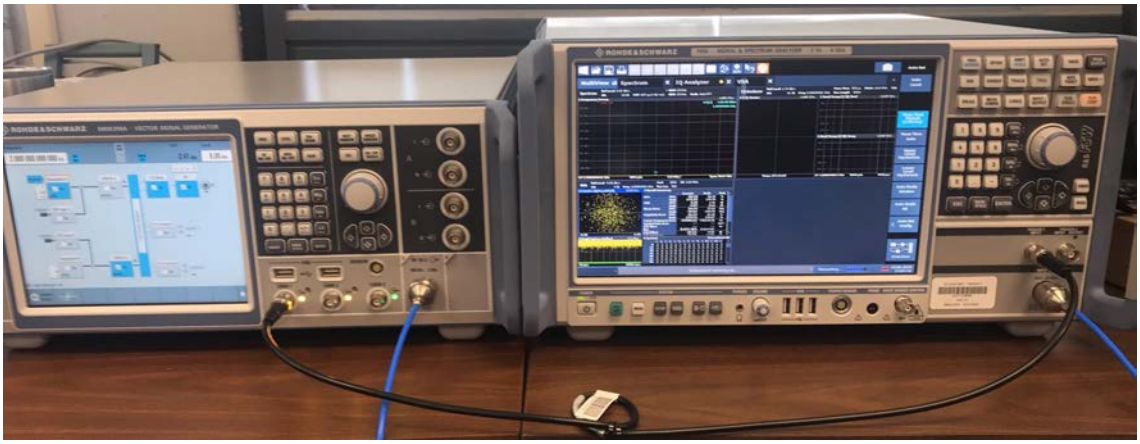

Figure 4.2. Physical test of radar embedded communications via cabled transmission.

As shown in Figure 4.2, a quick test to ensure that both signal generator and spectrum analyzer work properly is to simply send a RF sinusoid via shielded cable at some power

level and measure it with the spectrum analyzer. After that, actual shielded cable test can commence. The carrier frequency is set at 2 GHz with transmit power at 8 dBm. The received signal on the SpecAn is shown in Figure 4.3 when the radar-embedded communications is transmitted and received.

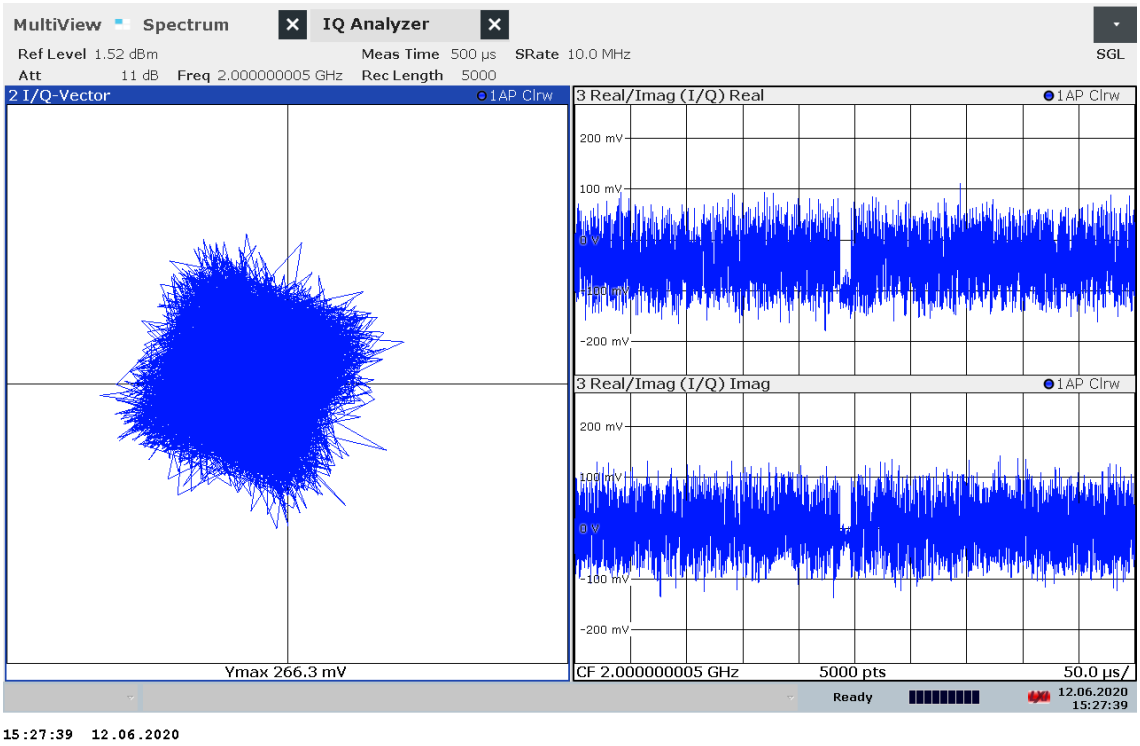

Figure 4.3. SpecAn screenshot of the pulsed radar embedded communications via cabled transmission

Although the constellation in Figure 4.3 appears static, initial measurements show that the constellation actually constantly rotates (with I and Q measurements constantly moving in time). This constant phase rotation is due to the frequency difference between the signal transmitter and receiver, which is a typical issue in radar and communications transmissions. In our implementation, the SigGen and SpecAn are eventually synchronized via reference clock signal from one equipment to another (although absolute synchronization is of course not feasible due to frequency drifts of the separate equipment oscillators).

After ensuring the received carrier signal and the I/Q data are correctly received, the received signal data is extracted from the SpecAn and loaded into the computer for

post-processing in MATLAB. Eventhough the two equipment are synchronized, there is instantaneous phase shift to the communications signal and not just the radar phase offset. This is simply due to the normal phase rotation in time. As such, a function is developed in MATLAB to adjust the shifted QPSK phases for coherent demodulation. The algorithm effectively takes the angle of the summed measurements such as to properly phase shift the constellation. The ambiguity as to which quadrant a particular symbol cluster belongs to is resolved by the zero-symbol sequence marker. The phase correction is shown in Figure 4.4.

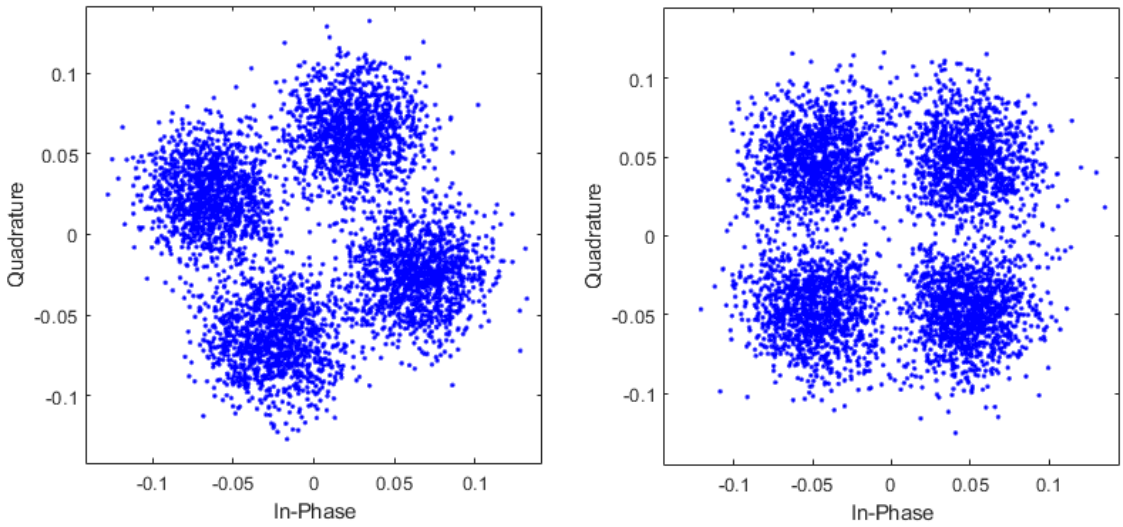

Figure 4.4. Received I/Q vector data with phase-shift (left), and adjusted coherent QPSK modulation (right)

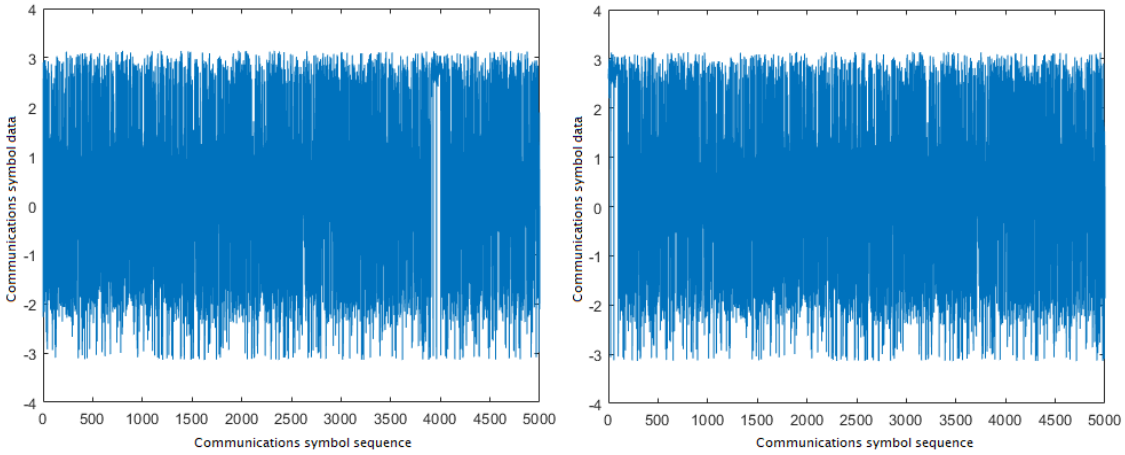

Figure 4.5. Received I/Q real data with sequence shift (left), and adjusted demodulated QPSK data sequence (right)

The adjusted coherent data set is used as input to both the MLE-MLD detector and DNN detector for demodulation. To avoid "one and done" transmission, the generator is set to keep repeating the transmission. On receive, the measurement time corresponding to the 5000 symbols being sent is set in the SpecAn. However, depending on when the data is taken, the start of the measurement can actually be anywhere within the 5000 symbols. In other words, the received symbols have to be lined up with the transmitted data sequence (as shown Figure 4.5). Then the received symbols data accuracy percentage for our detectors can be computed. Based on the 5000 communications symbols received, the MLD detector has a 98.4% correct symbol detection (i.e., SER of 0.016), while the DNN detector has a 94.1% correct symbol detection (i.e., SER of 0.059). This is in line with a 8 dB received SNR. Together with the QPSK phase offset error itself which is not in our original signal model, the received SER from both MLD and DNN detectors seem reasonable.

4.1.2 OTA Transmission Test

For the over-the-air testing, similar steps are followed as in the shielded cable test, with horn antennas installed on both the SigGen and the SpecAn for transmission and reception. The very large gain horn antenna is used as receiver front end to lower the SpecAn noise figure. Our estimate is it lowers noise figure to 4 dB. The distance between the antennas is about 3 meters to ensure far field approximation in a semi-controlled lab environment as

shown in Figure 4.6.

Figure 4.6. Bench OTA testing on pulsed radar embedded communications.

For the initial OTA test, we set the following: transmit frequency of the SigGen at 2.8 GHz, power at 20 dBm, RCR = 20 dB, and SNR = 30 dB, which results in adjusted received SNR = 26 dB. The received data from the SpecAn is reflected in Figure 4.7.

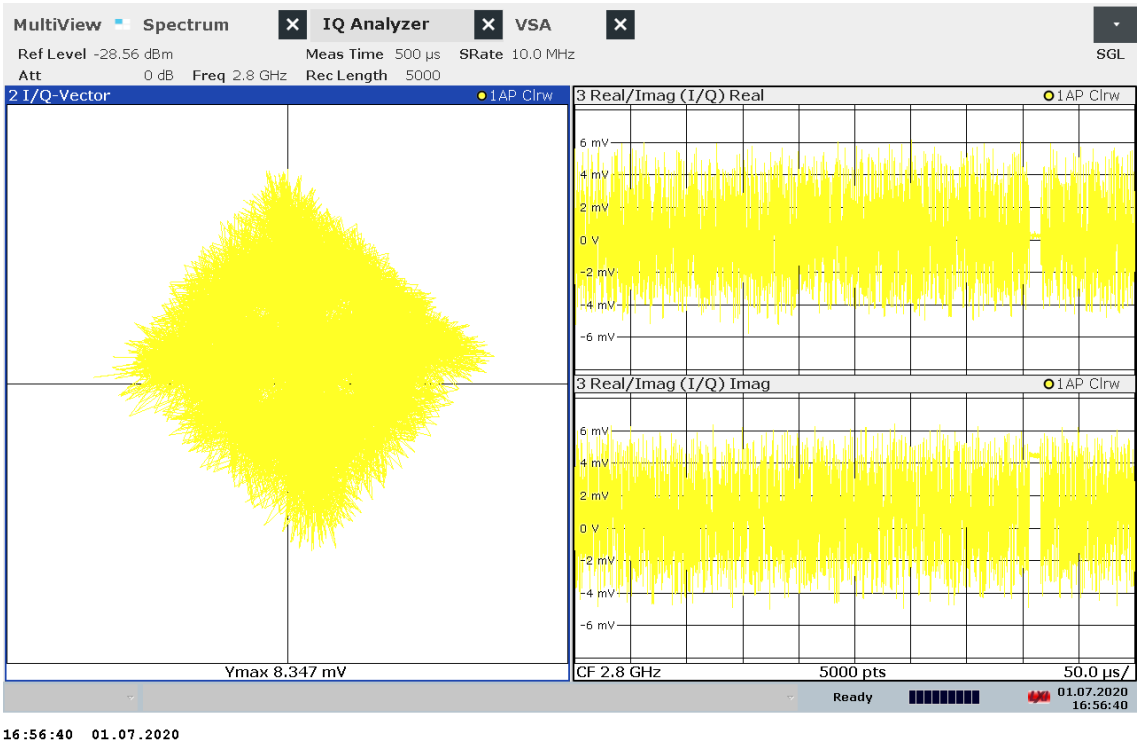

Figure 4.7. Constellation and IQ data of the received pulsed radar embedded comms (OTA)

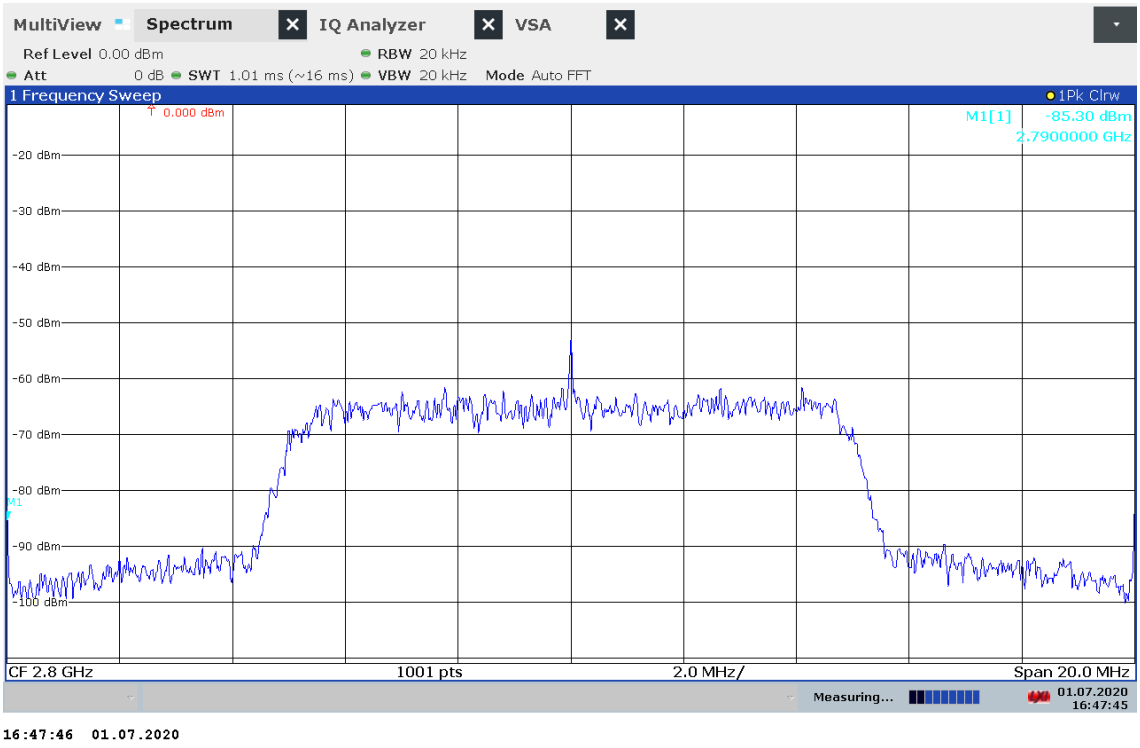

Figure 4.8. Spectrum of the received pulsed radar embedded comms (OTA)

A higher output power at 20 dBm is set, and antenna horns with greater than 20 dB are used at each end. The large SNR is confirmed in the SpecAn via Figure 4.8. This is clearly a higher SNR scenario compared to the shielded cable test.

The same phase offset adjustment and data sequence alignment need to be performed as before. The received raw and shifted data constellation are plotted in Figure 4.9 & 4.10 respectively, which clearly show a more tightened constellation and thus higher SNR. The MLE-MLD detector has a correct symbol detection of 100% (i.e., SER = 0), and the DNN detector has a correct symbol detection of 99.76% (i.e., SER = 0.0024) based on the 5000 data symbols received.

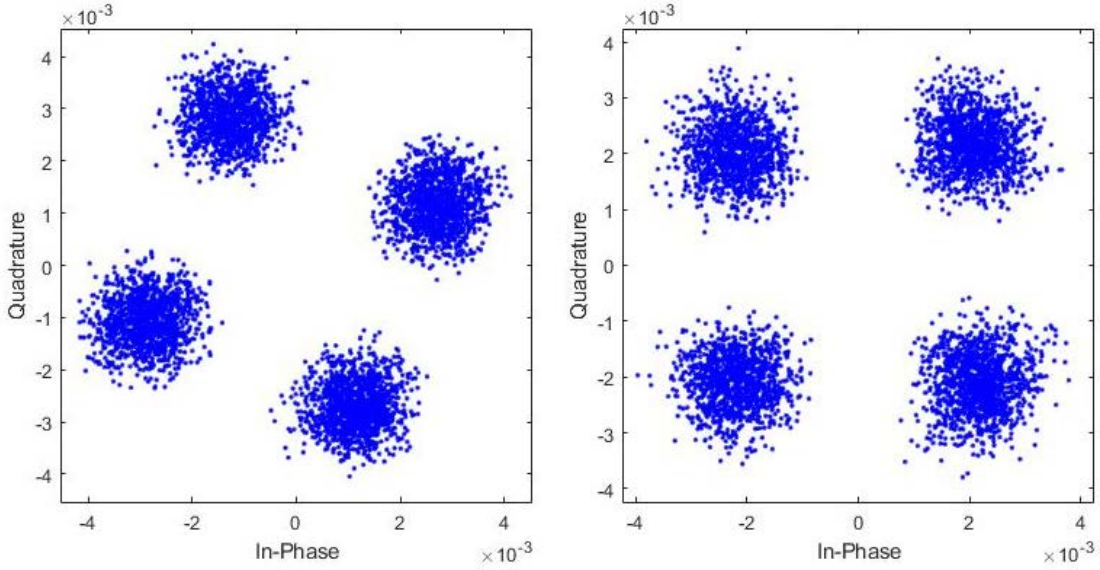

Figure 4.9. OTA received I/Q vector data with phase-shift (left), and adjusted QPSK modulation (right)

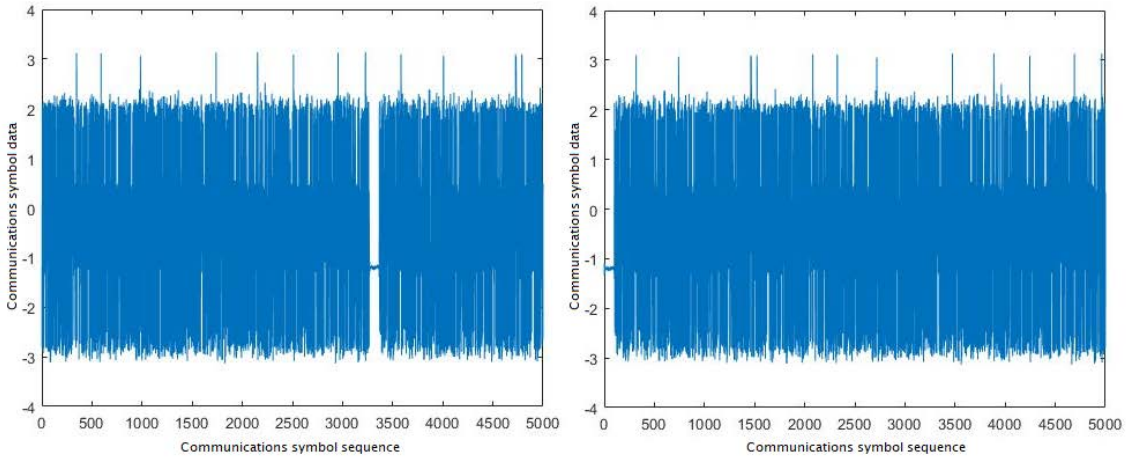

Figure 4.10. OTA received I/Q real data with sequence shift (left), and adjusted demodulated QPSK data sequence (right)

Subsequently, the OTA pulsed radar-embedded comms test is expanded, setting RCR = 30 dB, with various SNR (30, 25, 20, 15, 10 dB). The adjusted SNR and correct symbol detection percentage are reported in Table 4.1.

Table 4.1. MLD vs. DNN demodulation performance results for OTA pulsed radar embedded communications

SNR (dB)	30	25	20	15	10
Adjusted SNR (dB)	26	21	16	11	6
MLD correct symbol detection %	100%	99.58%	99.98%	99.98%	99.14%
DNN correct symbol detection %	98.89%	95.54%	94.36%	98.66%	96.86%

The MLD correct symbol detection percentages (1-SER) match the expected SER for adjusted SNR of 6, 11, and 26 dB. We would expect 100% correct symbol detection for 21 dB (and perhaps 16 dB). Notice however that there are only 5000 symbols sent (and not 1×10^6) and thus are not enough to get a good average detection result. In other words, one or two errors can easily skew results. Besides, the inherent instantaneous phase offset estimation (error from the post-processing algorithm) probably reduces the performance slightly.

While the DNN demodulator outperforms the MLD demodulator in the Monte Carlo simulations in MATLAB, the OTA lab measurements results indicate the opposite. This is mostly likely due to the communications instantaneous phase offset not being accounted for in the signal model and thus not accounted for in the ML training. Furthermore, the results obtained above are based on the neural network trained with simulated data as discussed in in Chapter 3. A neural network may potentially be trained with actual lab measurement data and communications phase offset, then the accuracy (or SER) of the DNN may outperform the MLD symbol demodulation accuracy (or SER).

4.1.3 Cross-Referencing of Detection Errors

After investigating the actual demodulated data, it is found that symbol errors made by the MLD and DNN demodulators do not completely overlap with one another. Take the adjusted SNR = 6 dB example in Table 4.1, the MLD demodulator has a correct symbol detection percentage of 99.14 with actual 43 errors out of the 5000 received symbols. The DNN demodulator yields a correct symbol detection percentage of 96.86%, with 157 errors out of the 5000 received communications symbols embedded in the radar signal (sample

demodulated data with errors is available in Appendix).

Comparing the demodulated errors together, it is found that out of the 43 errors in the MLD demodulation, DNN demodulator correctly demodulates 18. Unlike ML demodulation where the classification function in the output layer produces probabilities associated for each of the possible option for each symbol, once the MLD detection makes a symbol decision, there is no posterior probability in which to use with DNN to possibly use to improve detection. Though we can't improve the demodulation performance by simply combining the two methods since there is no error detection/correction implemented, a fact that the two detectors yield different errors is useful for cross-referencing of received symbols as well for investigating possible techniques for error mitigation.

4.2 LFM Radar Embedded Communications Test

For LFM radar embedded communications test, 5000 randomly generated QPSK communications symbols and noise are embedded into the LFM waveform to produce the .wv file from MATLAB to be loaded into the SigGen. One hundred zero-symbols are again inserted into the beginning of the comms symbols as marker. We initially set the RCR = 10 dB, SNR = 20 dB, and transmit frequency at 2.0 GHz, with power at 8 dBm for the shielded cabled test.

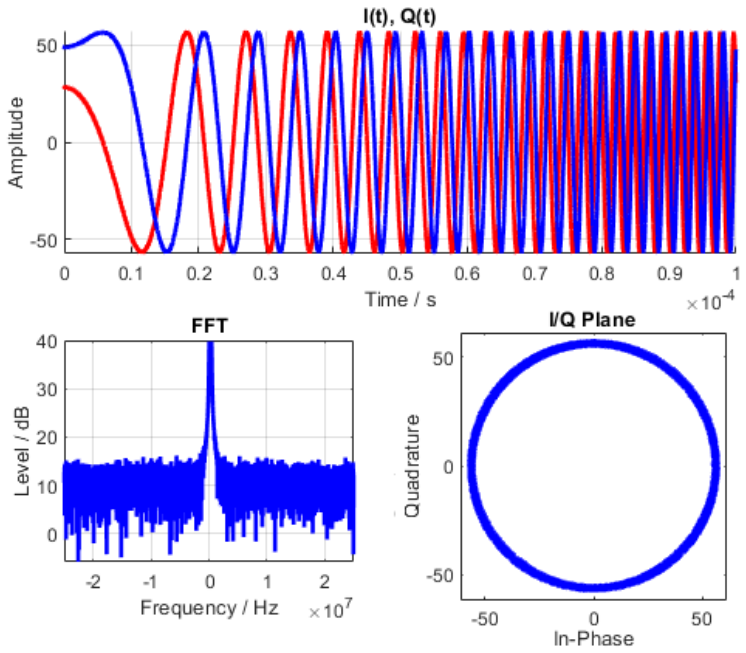

Figure 4.11. LFM radar embedded communications .wv file for physical signal generation

The received signal from the SpecAn is shown in Figure 4.12. The received IQ data is then extracted from the SpecAn and loaded into the computer. The same communications phase offset issue also exists in the LFM radar embedded communications and needs to be addressed. However, this time it is much harder to develop a straightforward algorithmic function to mitigate the phase offset.

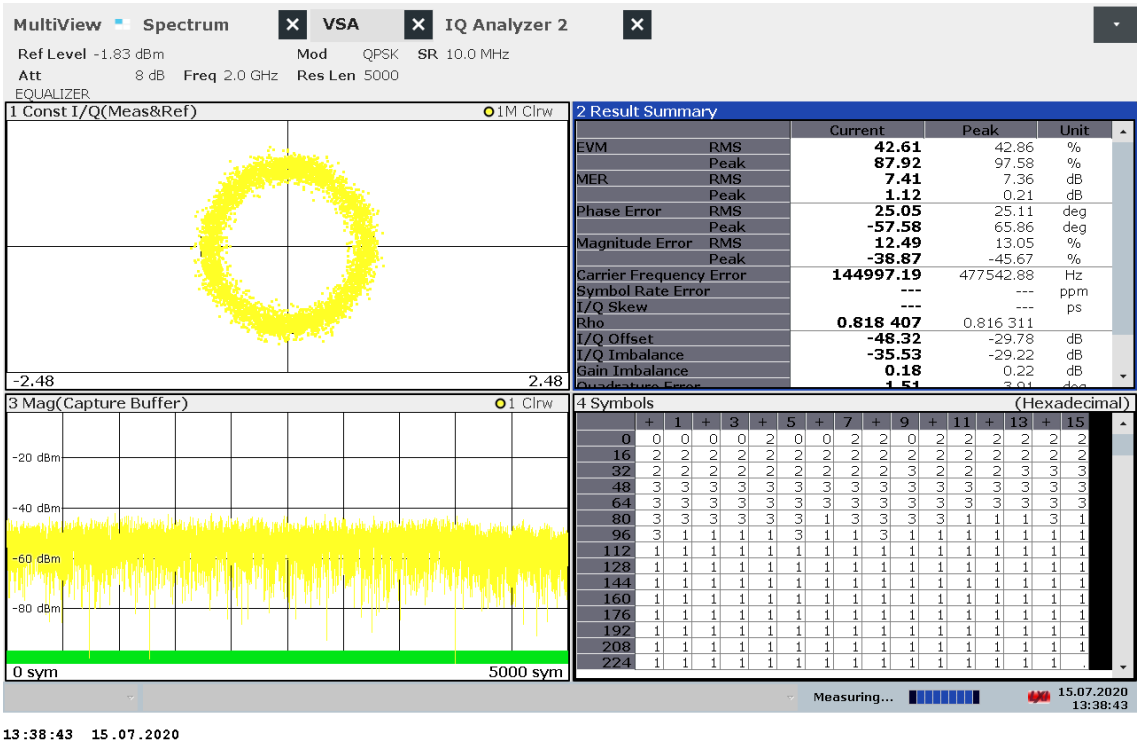

Figure 4.12. Multiview screenshot of the receiving SpecAn on LFM radar embedded communications

The circular IQ plot of the LFM waveform greatly differs from the resulting IQ constellation of the pulsed waveform-embedded QPSK and as such the instantaneous QPSK phase offset is difficult to estimate. Various attempts are taken to develop a function to mitigate the phase shift, but to no avail. This could be an aspect of future work for this research topic.

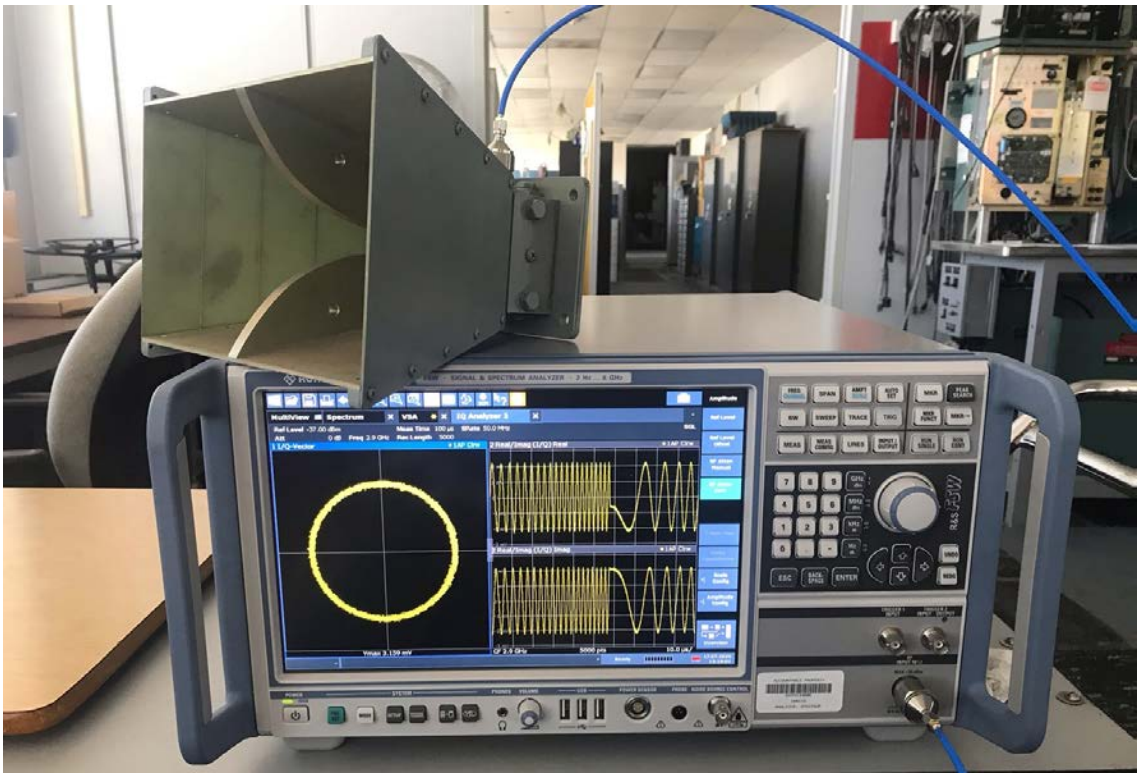

Figure 4.13. Receiving SpecAn of the OTA testing on LFM radar embedded communications

The OTA tests are still conducted for the LFM radar embedded communications, with RCR = 20 dB, SNR = 10 dB, transmit frequency at 2.9 GHz, and power at 20 dBm. As shown in Figure 4.13, the OTA test is successful, with the SpecAn displaying the received signal identical to our originally generated LFM comms signal. However, due to the communications phase offset problem, it is not possible for the MLD and DNN detectors to produce any meaningful demodulation results.

CHAPTER 5:
Conclusions and Recommendations

In radar-embedded communications, both radar and communications waveform interfere with each other and thus matched filter detection becomes suboptimal. Thus, in this work, machine learning demodulators are introduced to decode communications symbols that were embedded in a radar signal. Three versions of DNN demodulator were implemented for MPSK modulation. The DNN demodulators were compared to traditional matched filter or MLD MPSK detectors, which used MLE to estimate radar signal parameters such that the radar signal can be removed.

The 3 DNN demodulators used radar MLE in various ways. The first DNN version subtracted the radar estimate from the received signal and performed very close to MLD in terms of SER. The second one used the radar estimate as input to the training and performed slightly better in terms of low collection time N. The third DNN version was designed for varying values of RCR. Just like DNN version 2, it used raw received signal and radar estimate, with DNN training data RCR set to 28 dB for QPSK. This last version outperformed MLE-MLD in terms of SER. The DNN demodulator was tested for various values of RCR and proved to be robust for pulsed radar embedded communications.

The DNN demodulator was also applied to LFM radar embedded communications. In the case where there was no LFM phase offset, the DNN demodulator performed well in terms of SER much like the MLE-MLD. When the LFM phase offset was introduced, the DNN demodulator did well for low RCR but not large RCR. The MLE-MLD demodulator worked well to demodulate communications symbols embedded in LFM waveform even after the phase offset was introduced. For the machine learning DNN demodulator, perhaps a different approach and design of the neural network is needed in order to improve its performance in the presence of LFM phase offset.

In the OTA tests, both MLE-MLD and DNN detectors performed well in demodulating the communications symbols embedded in pulsed radar. In the LFM radar embedded communications OTA tests, no communications symbols could be demodulated due to the instantaneous QPSK communication phase offset that was difficult to mitigate. The receiv-

ing SpecAn properly received and displayed waveform that was identical to the originally generated signal. Therefore, from the simulations performed with LFM in Chapter 3, once the the phase-shift offset is correctly estimated, perhaps in future work, the MLD demodulator will be able to be utilized to take advantage of LFM radar embedded communications. Our objective would then be to apply it to satellites with SAR capability for SATCOM applications.

The neural networks in the OTA tests performed and described in Chapter 4 were trained with simulated data. For future work, real-world data should be collected and used to train the neural network for better results. Furthermore, real-world distortions such as temperatures, atmospheric effects, multipath propagation, and EMI interference can all be used as inputs for the machine learning training. The neural network can utilize these information to further improve machine learning demodulation (i.e., better SER) for radar embedded communications.

APPENDIX

A.1 OTA Demodulation Data

The following tables show the received demodulated data from the OTA testing on pulsed radar embedded communications as discussed in Chapter 4.1 with RCR = 30 dB, SNR = 10 dB, at 2.8 GHz, and power at 20 dBm.

The data below is chosen from the extensive tests and simulations for illustration, because it contains the previously mentioned 43 symbols that are demodulated erroneously by the MLD detector (out of 5000 transmitted symbols), alongside the DNN demodulated data for cross-reference.

Table A.1. OTA test demodulated data from pulsed radar embedded comms (Symbol Sequence No. 259..2078)

Seq No.	Originally generated data	MLD demodulated data	DNN demodulated data
259	4	1	1
689	1	4	4
747	4	1	1
1161	4	1	1
1254	1	2	1
1300	1	2	1
1458	1	2	1
1531	1	4	4
1639	2	1	1
1857	3	2	2
1858	1	2	1
1880	3	2	2
2027	4	3	3
2048	3	4	4
2049	4	3	4
2059	2	3	2
2078	3	2	2

Table A.2. OTA test demodulated data from pulsed radar embedded comms (Symbol Sequence No. 2127..4952)

Seq No.	Originally generated data	MLD demodulated data	DNN demodulated data
2127	4	1	1
2265	4	3	4
2343	3	4	4
2386	1	4	1
2403	4	3	4
2454	1	4	1
2536	3	4	4
3214	2	1	1
3223	1	2	2
3265	2	3	2
3272	4	3	4
3365	3	4	4
3522	3	4	4
3629	3	4	4
3747	2	3	2
3753	4	3	4
3770	1	4	4
3774	1	4	1
4178	4	1	1
4753	2	3	2
4788	3	4	4
4893	2	3	2
4895	3	4	4
4897	2	1	1
4924	4	1	1
4952	1	2	1

THIS PAGE INTENTIONALLY LEFT BLANK

List of References

[1] S. Blunt, “Intrapulse radar-embedded communications," *Air Force Office of Scientific Research No. FA9550-08-1-0167*, Lawrence, KS, 2011.

[2] S. Ma, J. Dai, S. Lu, H. Li, H. Zhang, C. Du, and S. Li, “Signal demodulation with machine learning methods for physical layer visible light communications: Prototype platform, open dataset and algorithms," *IEEE-Electrical Engineering and Systems Science - Signal Processing (eess.SP)*, Ithaca, NY, 2019.

[3] A. Mohammad, N. Reddy, F. James, C. Beard, “Demodulation of faded wireless signals using deep neural networks,” *IEEE 8th Annual Computing and Communication Workshop and Conference (CCWC)*, Las Vegas, NV, 2018.

[4] R. Romero, Y. Heng, T. Ha, “N-dimensional *M*-ary constant energy modulation for nonlinear communications channels,” *IEEE-APS Topical Conference on Antennas and Propagation in Wireless Communications (APWC)*, Granada, Spain, 2019.

[5] U.S. Air Force, "Space Radar Fact Sheet," Los Angeles Air Force Base, Los Angeles, CA, 2011.

[6] G. Meager, R. Romero and Z. Staples, “Estimation and cancellation of high powered radar interference for communication signal collection," *IEEE Radar Conference (RadarConf) 2016*, Philadelphia, PA, 2016.

[7] A. Hunt, "Various effects of embedded intrapulse communications on pulsed radar," M.S. Thesis, Dept. ECE, Naval Postgraduate School, Monterey, CA, 2017.

[8] A. Hunt, R. Romero, Z. Staples, "The effect of embedded intrapulse communications on pulsed radar probability of detection," *IEEE GlobalSIP Conference*, Anaheim, CA, 2018.

[9] G. Meager, “A high powered radar interference mitigation technique for communications signal recovery with FPGA implementation," M.S. Thesis, Dept. ECE, Naval Postgraduate School, Monterey, CA, 2017.

[10] M. Richards, J. Scheer, W. Holm, “Principles of modern radar," *SciTech Publishing*, Raleigh, NC, 2010, ISBN: 978-1-891121-52-4.

[11] P. Kim, “MATLAB deep learning with machine learning, neural networks and artificial intelligence,” *Apress*, 2017, ISBN-13:978-1-4842-2845-6.

[12] B. Wade, “Machine learning for aerospace applications," Army Research and Analysis Center, Monterey, CA, 2019.

Initial Distribution List

1. Defense Technical Information Center
   Ft. Belvoir, Virginia

2. Dudley Knox Library
   Naval Postgraduate School
   Monterey, California